7-2018

Assessing the tensile and fatigue behavior of aerosol jet printed nano silver particle traces on polyimide substrates

Roshan Muralidharan
Binghamton University--SUNY, rmurali2@binghamton.edu

ASSESSING THE TENSILE AND FATIGUE BEHAVIOR OF AEROSOL JET PRINTED NANO SILVER PARTICLE TRACES ON POLYIMIDE SUBSTRATES

BY

ROSHAN MURALIDHARAN

BACHELORS IN ENGINEERING, PES INSITITUTE OF TECHNOLOGY
BANGALORE, 2011

THESIS

Submitted in partial fulfillment of the requirements for
the degree of Master of Science in Industrial and Systems Engineering
in the Graduate School of
Binghamton University
State University of New York
2018

Accepted in partial fulfillment of the requirements for

the degree of Master of Science in Industrial and Systems Engineering
in the Graduate School of
Binghamton University
State University of New York
2018

July 31st, 2018

Dr. Peter Borgesen, Professor and Faculty Advisor
Department of Systems Science and Industrial Engineering, Binghamton University

Dr. Nagendra N Nagarur, Committee Member
Department of Systems Science and Industrial Engineering, Binghamton University

Dr. Changqing Cheng, Committee Member
Department of Systems Science and Industrial Engineering, Binghamton University

Abstract

Flexible interconnects are integral to flexible hybrid electronics. Aerosol jet, inkjet or screen printing offer various advantages and disadvantages compared to electroplating, but the behavior of printed metal traces under various types of loading is very different and not yet well understood. This thesis presents an assessment of the electromechanical behavior of aerosol jet printed Nano silver particles on two common polyimide substrates, Upilex and Kapton.

There are many different aspects to electromechanical testing of flexible interconnects, but this work focuses on the effects of tension and cyclic loading. In comparison to the much more widely researched electroplated copper or vapor deposited silver traces, AJP traces exhibit a stronger increase in electrical resistance for comparatively minor strains and they damage much faster under cyclic loading conditions. The fatigue behavior is seen to vary with the combination of substrate modulus and viscoelastic deformation properties. The rate of damage increases faster with increasing amplitude on the less compliant substrate and, consistently with this, raising the minimum strain in the cycle led to a significantly stronger reduction in damage rates. However, the damage rate remained lower on the less compliant substrate at all amplitudes considered.

Acknowledgments

I would like express my deepest gratitude to my advisor Dr. Peter Borgesen. This work materialized only because of his patience, consistent guidance and scientific expertise. I would also like to thank Dr. Nagen Nagarur and Dr. Changqing Cheng for their willingness to be part of my thesis committee and in providing their valuble insights for the betterment of my research.

A special note of thanks to Dr. Mark D Poliks and his team for providing me the opportunity to work with NextFlex project.

I am grateful to my research team members Rajesh, Manu and Maan for the extensive guidance in setting up the experiments and analyzing data. I would also like to thank Nardeeka, Sanoop, Arun, Jorge, Thaer and Ashwin for all the help extended to me in the lab.

Finally, I would like to thank my parents for their encouragement and support in all my endeavors.

Table of Contents

List of Figures

Chapter 1 Introduction

With ever increasing demand for newer and challenging electronic technology the industry sees huge potential in flexible hybrid electronics. Flexible electronics, as the names suggest, are expected to allow for higher mechanical flexibility along with good conductivity. Flexible hybrid electronics includes conventional electronic components on flexible substrates that have conductive traces connecting them [1]. The conductive traces may be formed by an additive manufacturing process/printing. Types of printing include screen-printing, gravure printing, ink jet and flexographic printing used to fabricate flexible electronics.

Thin conductive metal films of copper and silver can be bonded on to polyimide substrates such as Upilex™ and Kapton™. Such printed metal films form the electrically conducting interconnects that could be used in manufacturing of flexible hybrid electronics. Key to understanding the performance and the service life of these flexible hybrid electronics would be to understand the performance in mechanical testing and accelerated aging tests. The mechanical aspect of testing includes performance of interconnects, while they are being stretched, bent and under fatigue. Accelerated environmental testing includes measuring the performance of the interconnects after accelerated aging in thermal cycling, annealing and exposure to humidity. We use the resistance measured across the trace as a parameter to determine the performance of these interconnects. The reason we are interested in the resistance measured across the trace is;

1) the primary function of the trace is to conduct, so we care when it conducts less well, and 2) the strength of the trace can't be measured because measured loads are dominated by the substrate.

1.1 Assessment of electromechanical behavior of electroplated copper trace on polyimide substrate.

The behavior of electroplated copper on a Kapton substrate in tensile testing has been well studied. We know that free standing metal films deform plastically when subjected to significant tensile loading. When stretched a free-standing film forms a neck, where the strain is then much higher than elsewhere in the film, thus demonstrating strain localization and subsequent failure at relative small average strains [2].

Electroplated copper traces on Kapton, unlike free standing copper films, can sustain higher strains when subjected to mechanical stresses such as when being stretched. The substrate prevents strain delocalization, when adequately bonded, enabling the trace to be stretched close to the failure of the substrate[3]. Lu et al (2007) have demonstrated that electroplated copper on Kapton will conduct until up to the failure of the substrate. Conducting a similar experiment, we measured the resistance of an electroplated copper trace on a 2 mil (approx.) Kapton substrate, subjecting it to stretching at constant strain rate. The trace is 60mm in length, 150μm wide and 6μm thick. We observed continuous resistance increase while being stretched until 35% (Figure 1.1).

The resistance of the trace, measured in-situ using a 4-wire method, increased when it was being stretched under tensile loading using a single column Instron universal tensile

machine. The ratio of resistance (R) of the stretched film to the initial resistance (Ro) observed experimentally scales with the well-established relationship, Equation 1:

$$R/Ro = (L/Lo)^2 \qquad (1)$$

Ro= Initial resistance of the trace

R = resistance of trace when stretched

Lo = Initial length of the trace

L = overall length of the trace when stretched

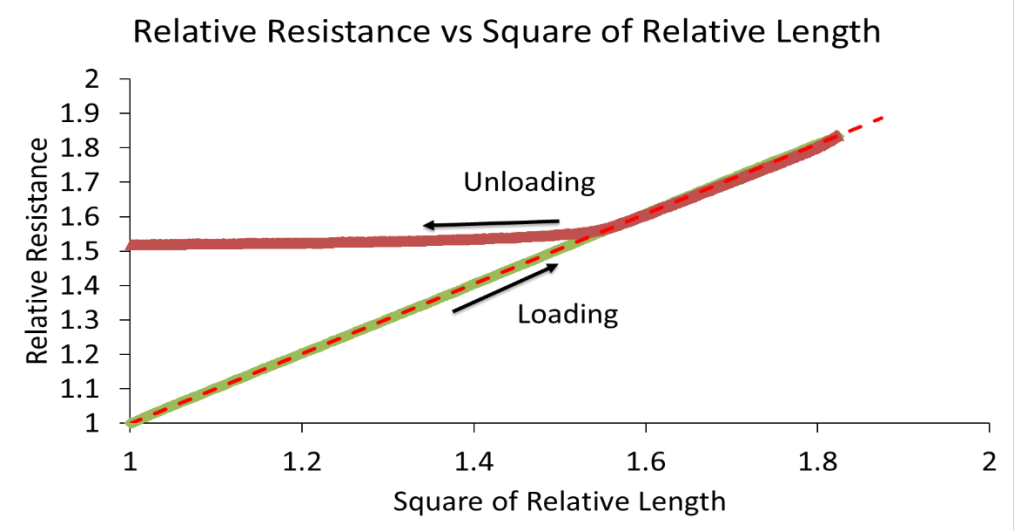

Figure 1.1 Relative resistance to square of relative length for electroplated copper trace on Kapton

The above relationship assumes that there's no significant change in the volume and density of the film and the resistivity remains unchanged. Thus, the resistance of the trace can be represented by $R=\rho L/A$, where R is the resistance of the trace, ρ is the resistivity of copper, L is the length at the instance and A is the cross-sectional area of the

trace. This suggests that the change in resistance is due to the elongation of the trace along with the substrate together with the lateral shrinkage required to preserve the trace volume and that there are no cracks in the trace or delamination of the trace from the substrate.

On releasing the load, the relative resistance value follows the same curve as during loading till a certain point, after which it deviates and levels off at a much higher value than what we started with. At that point the sample goes slack, and the Instron reads zero load all the way until the cross head reaches the initial position. This indicates that the sample has deformed and is now longer than what we started with, restricting the trace from returning to its original length and increasing the resistance of the sample. The deformation of the polymer substrate is partly recoverable over time and partly permanent. The recoverable deformation is called viscoelastic deformation and the permanent deformation, plastic. The elevated resistance values, at the point where the Instron reads zero is due to the viscoelastic strain maintaining a longer trace length. The fact that the resistance at a given strain was the same during loading and unloading, and that it varied with the square of the relative length, until then shows that there was no damage to the trace.

1.2 Aerosol jet printed nano silver traces on polyimide substrates

Like electroplated copper traces aerosol jet printed nano silver traces on polyimide substrates are composed almost only of metal. Their porous structure means that the effect of stretching even without damage is not quite the same, but we still use the relationship between relative resistances with the square of relative length as an approximation to help understand the behavior of aerosol jet printed traces. Nano silver traces were aerosol jet printed on Kapton and Upilex substrates. We use nano silver because, good printing with

nano copper has not been established yet, silver oxide conducts, the silver ink bonds with polyimide and silver has better conductivity than copper. Both the substrates have different mechanical and physical properties.

The samples are formed on a 2 mil thick DuPont™ Kapton® HN polyimide film or UPILEX®-S 50S polyimide substrate with 2 layers of aerosol jet printed nano silver ink. The surface of the traces are porous on both substrates (Figure 1.2)

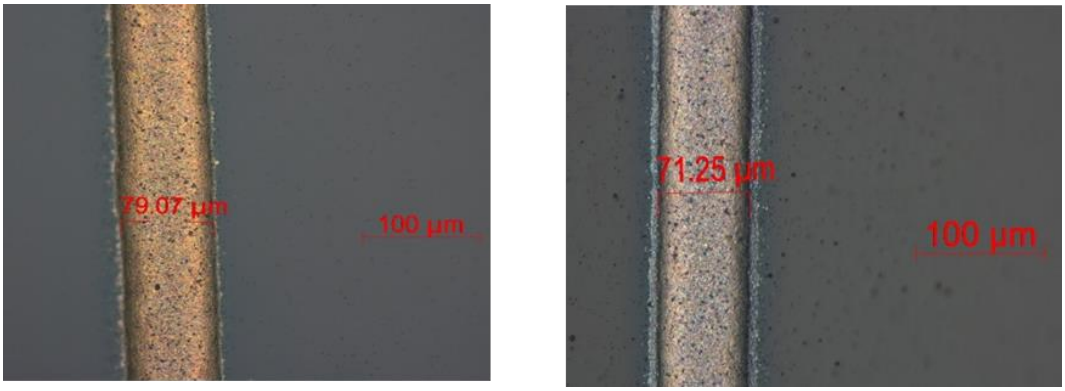

Figure 1.2: Nano silver trace on Upilex (Left); Nano silver trace on Kapton (Right)

1.2.1 Mechanical difference in the substrates

The two substrates have different mechanical properties. Bare substrates were stretched until failure. The tensile modulus and tensile strength observed match with the specification values. The data sheet specifies tensile moduli for Kapton and Upilex as 2.5 GPa and 9.3 GPa, respectively. The load-displacement curves (Figure 1.3), show Upilex to be stiffer than Kapton. In a practical application, Upilex may thus resist stretching more so that it is stretched less.

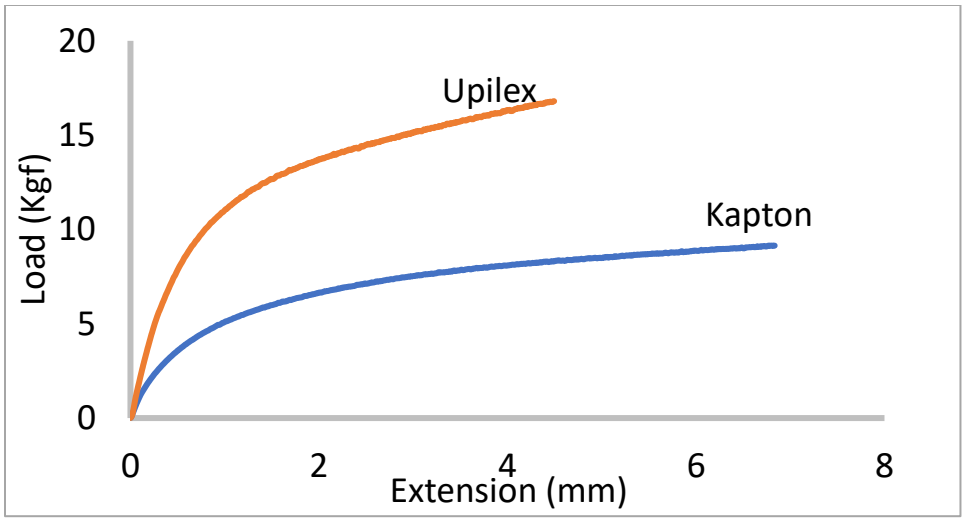

Figure 1.3: Upilex and Kapton bare substrate tensile test

In sections to follow we will look at the electro-mechanical differences for traces printed on these two substrates under various testing conditions. Chapter two describes the general methods of printing flexible traces on various substrates. It also illustrates some practical applications for aerosol jet printing. The rest of the chapter provides a brief account of the general back ground and the research conducted pertaining to aerosol jet printed traces. Chapter three describes the experimental procedure, sample specifications and parameters. It also gives a description on the equipment used, its specifications and operating procedures. Chapter four discusses the results based on the experimentally observed finding and differences, and proposes plausible underlying mechanisms. Chapter five summarizes the work done and provides an outline of proposed future research.

Chapter 2 Literature Review

2.1 Printing Methods

Technological advancements in electronic devices and their associated process are inclined towards low cost, low weight and large area integration of the devices. Flexible electronic devices meet these demands with their low density, enhanced stretchability, long term reliability and smaller foot print on the environment. A flexible PCB for example takes only about 10% of the space and weight, and it involves no chemical etching as compared to its rigid counterparts. Besides that, its bend capabilities makes it a viable option for wearable tech, flexible displays, thin film solar cells, aerospace and military applications, and medical applications also. Most flexible electronics involve the use of polymeric substrates with metallic film traces electroplated or printed on them. Traces are commonly printed using additive manufacturing methods layer by layer. Common printing methods in use today are gravure, offset lithography, flexography, screen printing and direct write methods such as inkjet printing and Aerosol jet printing.

2.1.1 Gravure printing

Gravure printing is a roll to roll printing method. It uses a rotating cylinder or a plate engraved with a desired pattern to directly transfer conductive ink on to a flexible substrate. The substrates are usually paper like materials or fabrics. Harder substrates such as alumina and glass substrates are also printed using this method. The substrate is forced

between the impression roller and the engraved cylinder (Figure 2.1), allowing for transfer of ink from the cylinder to the substrate by capillary action.

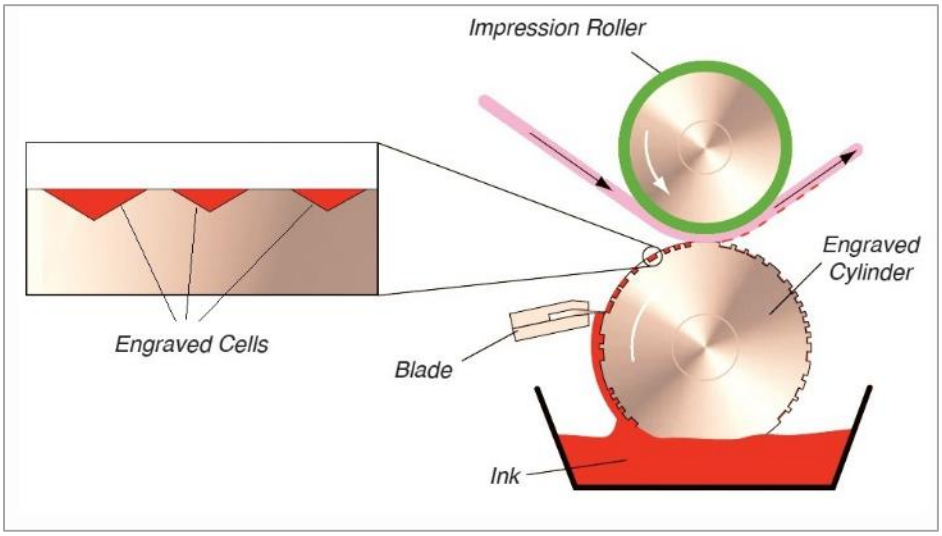

Figure 2.1: Roto-gravure printing[4]

The engraved spaces hold the ink; the depth and the width of the groves are the control parameters for the trace dimensions and quality. The inks are specifically formulated particulate polymers called electrically conductive adhesives. The particle shapes are also given specific considerations to enhance the ink rheology. The advantage of gravure printing lies with its ability to print large surface areas in a very short time. The limitation arises often with repeatability when the grooves are blocked with the ink [5].

2.1.2 Screen printing

Screen printing is widely used in textile and surface mount technology for application of solder paste. It is carried out by spreading out and squeegeeing conductive ink through a screen directly onto the substrate. The screen has the desired circuit pattern selectively etched using photo lithography. The screen is then lifted off and the conductive ink is cured by either heat or UV light [6].

Screen printing is presently the most widely used technology for commercial applications of printed electronics (Figure 2.2). Screen printing is often limited by the resolution for finer prints but there's research being driven in the direction to print sub 20-micron level [7]

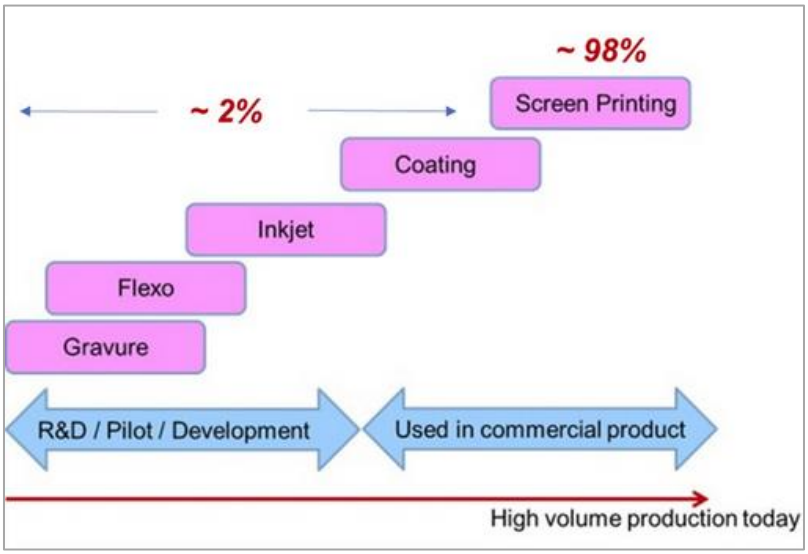

Figure 2.2: Distribution of printing technology for commercial applications[7]

2.1.3 Inkjet printing

Inkjet printing is a direct write printing method, it was a well-known and applied technique in graphical printing that was later extended to printing electronics. Direct write methods such as inkjet printing and aerosol jet printing have the following advantages over other printing methods:

i) A broad spectrum of materials may be used as substrates

ii) CAD aided manufacturing

iii) Higher precision

iv) No masks required, allowing for 2D and 3D printing applications

v) Higher material utilization

Inkjet printing can be classified into 4 categories based on the technology used; piezo ink jet printing (Figure 2.3), thermal ink jet printing, electrostatic printing and acoustic ink jet printing [6].

The ink droplets are dispersed from the reservoir using any of the 4 methods mentioned above and are guided on the substrate using a charged electrode.

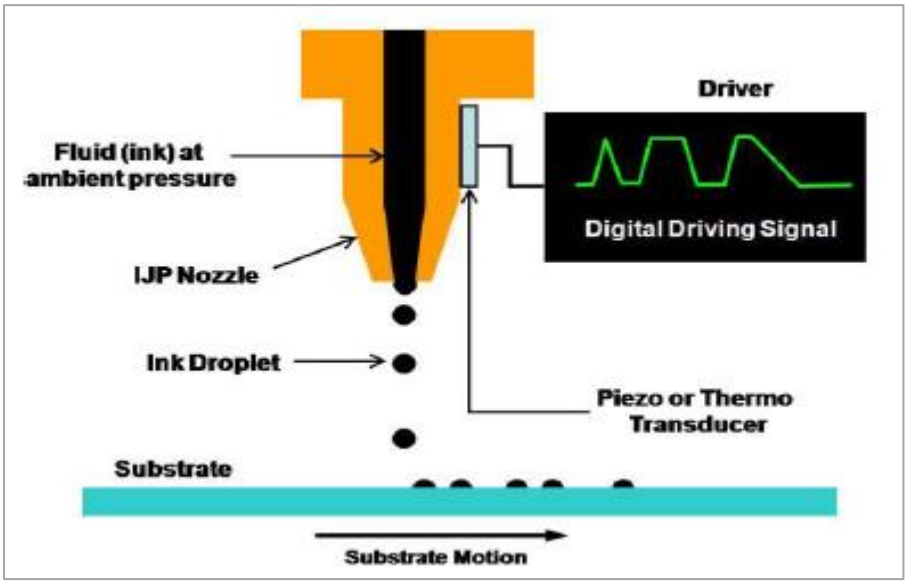

Figure 2.3: piezo electric ink jet printing [6]

The scope of inkjet printing is limited by the types of inks used, its formulations and viscosity. One of major issues, clogged heads, often result from changes in the ink composition and evaporation at the nozzle. Another critical parameter governing the printing process is the selection of a suitable printing head, which in turn would ensure good jettablity, stability of the ink droplets on the substrates and avoid satellite drops [8].

2.1.4 Aerosol jet printing

Aerosol jet printing is a relatively newer additive manufacturing printing technique driven by CAD. It has several advantages over ink jet printing. It can work with a wider range of functional materials such as conductors, resistors, di-electrics with inks consisting of metals, polymers, ceramics and even bio-materials. In principle it uses aerodynamic focusing using a sheath gas to deposit the ink on the substrate. The ink is placed in an atomizer, which could be an ultrasonic or a pneumatic atomiser depending on the ink used and its viscosity. The atomised mixture is carried over by the gas flow to the disposition head. In the head, the sheath gas forms an annular ring to direct the atomised mist on the substrate [8]. This process allows fine droplets of diameter of 1-5 µm to be impinged on the substrate at speeds of almost 80m/s. The sheath gas is dry clean N2. The small size of the ink droplets allows for fine features (10 micron) to be printed with clean edges. Depending on the material deposited the thickness of the deposited trace can be controlled from 25nm to several microns

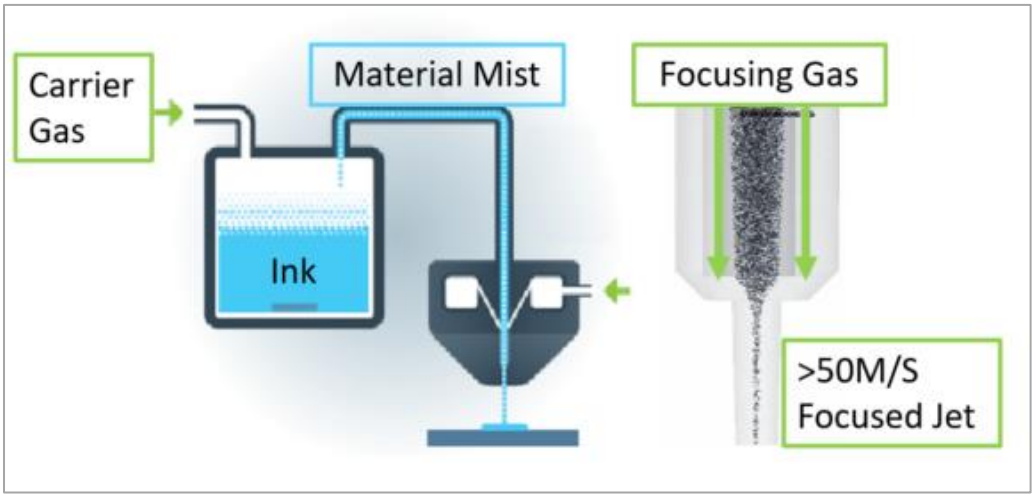

Figure 2.4: (Left) Aerosol jet printing, (Right) nozzle[8]

The overall process (Figure 2.4) is relatively clean and since there's no contact of the ink anywhere during the process it helps avoid clogging and materials build up in the heads. Aerosol jet printing also allows for printing with inks over a large viscosity range (0.7- 2500 cP). However, further processing is required of the inks, for e.g. metallic inks often have to be sintered. Manufacturers often claim the printing quality to yield near bulk resistance properties for metallic inks used for electrical applications. The metallic inks used include Nano particle silver, gold, platinum and palladium inks. The parameters that influence printing [9] are listed in Figure 2.5. Recent developments in aerosol jet printing also allows for multi axis 3D printing for applications such as molded interconnect devices.

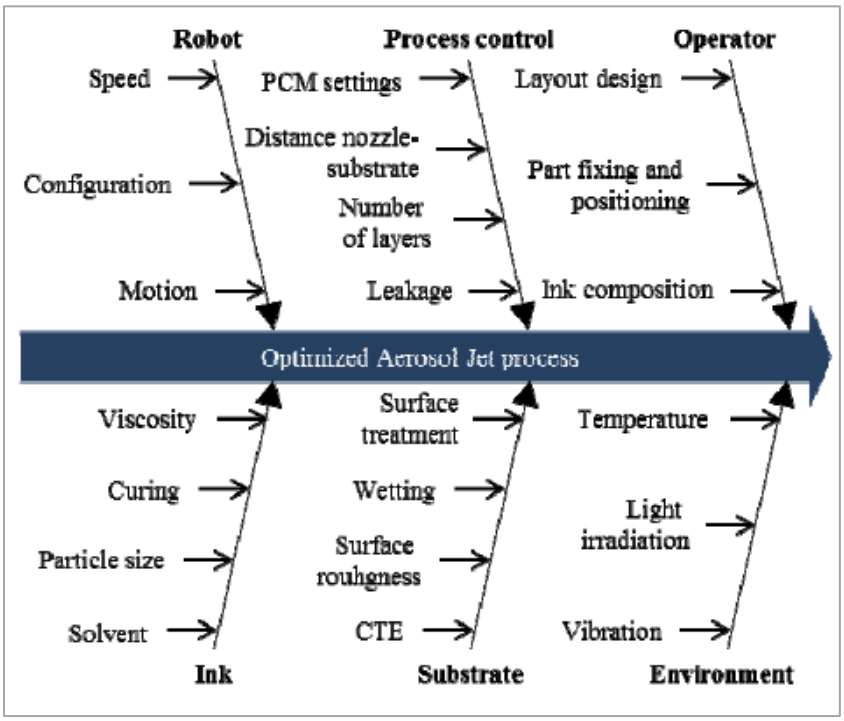

Figure 2.5: Process parameters influencing aerosol jet printing process [9]

2.2 Practical application of aerosol jet printing

Marinov et al. (2007) used aerosol jet printing to print silver traces for use as chemisensors or vapour sensors. Chemisensors are important in medical and food industries to detect chemical agents. In these sensors a polymer sensitive to the gas along with carbon black would be coated on disjoined silver traces. The polymer would swell on exposure to the nerve gas simulant such as dimethyl methyl phosphonate (DMMP), thus functioning as a sensor. If not for the recovery time after exposure, the direct writing method proved to be viable option as a sensor[10].

Maiwald et al. (2009) fabricated sensors for non-destructive applications in areas like structural health monitoring using a aerosol jet printing process. The sensor is a multi-layered structure beginning with a CAD drawing, followed by deposition of a polymer isolation layer, a nano silver layer and an encapsulation to protect the sensor all directly built on a metal surface (Al). The resulting metal layer demonstrated high electrical conductivity up to 70% of its bulk value after thermal curing. The strain gauges were compared against commercially available strain gauges, and showed good reliability and repeatability over a number of cycles [11].

Jones et al. (2010) have demonstrated fabrication of High-speed SWCNT (single-walled carbon nanotubes) based flexible FE-TFTs (field effect thin film transistor) using aerosol jet printing technology. The SWCNT are excellent candidates for fabricating flexible electronics. Owing to the fact that the aerosol jet printing is capable of printing fine structures with high precision, researchers have printed the design of a top gated field effect thin film transistor (FE-TFT) using this medium on a Kapton substrate. Offering

better performance than their organic counterparts, the resulting SWCNT based FE-TFT has been described as a start for fabricating low cost high speed flexible electronics [12].

Clifford et al. (2018) have put forth the idea of printing sensors on integrated chip devices. They have demonstrated this by fabricating a humidity sensor that uses a combination of disjoined printed silver traces along with a film of Nafion, a humidity sensitive layer [13]

Optomec has demonstrated smart phone and other consumer device antennas made with aerosol jet printing owing to 3D printability [14].

2.3 Research on electromechanical properties of printed traces

Lu et al. (2007), demonstrated introduction of a Cr layer to improve adhesion of electrodeposited Copper on Kapton. Copper has poor adhesion to polyimides even after the polyimide surface has been treated with plasma. A thin layer of chromium when deposited reacts with PI at the interfaceforming a uniform layer. Electrodeposition of copper on this chromium under layer leads to better adhesion and in turn suppresses strain localization thus increasing the rupture strain. They observed that the electrical resistance of the sample when stretched increases and the change in relative resistance agreed with theoretical predictions made under the assumption that the film retains its rectangular shape. They reported that they have not seen any cracks until 40% strain, found occurrence of micro-cracks at 50% strain and indicated that the sample finally fails by a ductile mechanism involving coevolution of strain localization and debonding [3].

Suo et al. have summarised the research being done to understand the mechanics of thin inorganic films on flexible hybrid structures. The constituents, owing to their small

features and hybrid materials behave differently from their bulk counterparts. They base their findings on the two facts that could allow inorganic materials to be flexible, i.e.

1) Sufficiently thin substrates supporting thin inorganic films, by the virtue of elementary beam theory experience small bending strains

2) The small flaw size enables inorganic films to sustain higher strains.

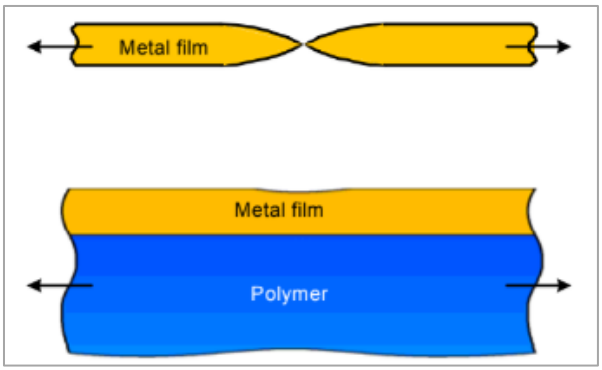

Figure 2.6: (Top) necking in a free-standing film, (Bottom) metal film on a polymer substrate [15]

On the contrary, examining the ductility of thin free-standing metal films when sufficiently stretched showed rupture due to localised necking (Figure 2.6). This local elongation of the film is constrained when the film is bonded to a substrate [15].

Xiang et al (2005) have demonstrated that the rupture strains of thin metal films on polymeric substrates is sensitive to their adhesion. Comparing two extreme cases, one involved Cu films deposited on 125μm thick Kapton with a carbon release layer which resulted in channel cracks being formed at 2% tensile strain. The poor adhesion also resulted in peeling of the Cu films between adjacent cracks. In the second case, adequate bonding of the Cu to the substrate was ensured by depositing on a Ti under layer. This resulted in no visible cracks up to a strain of 10% and micro cracks at 30% strain due to local thinning and intergranular fracture [16].

Li et al. (2004) have demonstrated that the substrate can suppress strain localization using finite element simulation. They have concluded that the stiffness of the substrate plays a vital role in suppressing the elongation of the metal film under tensile stretching. Metal films on extremely compliant substrates, with Young's modulus in the range of 2 MPa, when stretched form a single neck in the film, and the films ruptured at strains comparable to the rupture strains of a free-standing film. On the other hand, metal films on moderately stiff substrates (100-150MPa) such as silicone with a Cr under layer to improve adhesion, form multiple necks on being stretched, thus surviving higher strains. For metal films on stiff substrates such as polyimide (~ 3GPa), with adequate adhesion were found to rupture at significantly larger strains [17].

Researchers have found that for certain conditions the substrate is ineffective in restricting the strain localization. For example Z. Suo et al. (2005) have found that there's a variation in how much strain a well bonded Cu film can sustain. Theoretically if the adhesion is good, the Cu film should be able to survive up to the failure of the substrate. But experimentally it was found to be only in the range of 10-30%. The reason for this variation has been attributed to

1) The small grain size of the films imposed a constraint on dislocation motion or the presence of trace impurities segregating into the Cu boundaries, leading to excessive stresses and intergranular fracture in the films.

2) Co-evolution of debonding and strain localization when stretched [15].

Xiang et al (2005) have elaborated on the co-evolution of debonding and strain localization. When stretched, the Cu films first undergo uniform deformation, and there is no significant traction exerted by the Cu film on the substrate. However, when the strain

increases, imperfections in the Cu film may initiate strain localisation, thus arousing traction at the film substrate interface. This could lead to delamination, if the adhesion is poor and subsequent failing due to necking.

Alternatively, strain delocalization is also explained in terms of dislocations. For a free-standing film or a poorly bonded film to the substrate, the dislocations have no restraint causing more and more dislocations to spread allowing for strain localization [16].

Thus for strong interfaces with a hard and a stiff material, there would be an effect of plasticity of metal films. The dislocation movement is restrained and hardening increases. Z. Suo et al (2005) speculate that, in the case of interface with a softer material or a weaker interface, the dislocation might reach the interface and pile up causing slip steps or debond from the interface. These slip steps and the initial instances of debonding may acts as sites for interfacial cracks initiating delamination and strain localization [15]

Sim et al. (2011)**,** have demonstrated the effect of good adhesion of deposited Ag on PET substrate in terms of electrical performance under tensile strain. They have compared the performance of Ag deposited on PET with an acrylic under layer to Cu deposited on PI with a Cr under layer, both being subjected to tensile testing. Ag on PET samples showed better adhesion, having a higher failure strain of 70% as compared to the 60% strain for Cu on PI samples. This also resulted in better electrical performance and the failure was by strain localization and cracking associated with defects [18].

Mei Et al have used a relationship established by Beuth (1992) for the energy release rate for a steady state growth of a channel crack in a thin film on an elastic substrate as :

$$G_{ss} = Z(\alpha, \beta)\frac{\sigma_f^2 h_f}{\bar{E}f} \qquad (2)$$

where σ_f is the stress on the film, h_f is the thickness of the film, $\bar{E}_f = E_f/(1-\upsilon_f^2)$ is the plain strain modulus of the film with Young's modulus E_f and Poisson's ratio υ_f. Z, the crack driving force depends on the elastic modulus of the substrate and the film through α & β, called the Dunder's parameter.

Where $\alpha = \frac{\bar{E}_f - \bar{E}_s}{\bar{E}_f + \bar{E}_s}$ and

$$\beta = \frac{\bar{E}_f(1-\upsilon_f)(1-2\upsilon_s) - \bar{E}_s(1-\upsilon_s)(1-2\upsilon_f)}{2(1-\upsilon_f)(1-\upsilon_s)(\bar{E}_f + \bar{E}_s)}$$

The value of Z decreases for a compliant film on a relatively stiff substrate and increases for a film on a more compliant substrate [19][20].

Based on equation (2), Vlassak (2003) predicted that the crack driving force Z varies linearly with the modulus of the substrates for the present combinations of substrate and trace dimensions [21].

Sim et al. (2012) have conducted studies on comparing the tensile and fatigue behaviour of micro gravure printed nano particle (NP) sized silver ink and electroplated silver on PET substrate. An acrylic primer was used to improve adhesion in both cases. Films of thickness 100nm and 380nm were printed. In-situ resistance measurement during uniaxial tensile tests of 100nm thick films samples showed comparable failure strains for both types of printing. For the conditions defined by them, the failure strains were 4.7% and 4.3% for electroplated and NP respectively. The mode of failure is reported to be due to intergranular cracking, owing to the size constraint (100nm). The 380nm thick NP sample performed poorly when stretched, which they attributed to high porosity leading to loss of electrical connection at a strain of 3%. The fatigue life of 100nm thick sample

printed by NP and electron beam evaporation is comparable. They conclude by saying that owing to its process advantages, NP printing despite its performance limitations could be a good alternative to printing ultra-thin films on polymers [22].

Sim et al. (2012) conducted experiments to determine the fatigue performance of thin silver films deposited by electron beam evaporation on a 12μm thick PET substrate. They have compared the fatigue life with and without an acrylic primer under layer to improve the adhesion. Under these conditions they have reported two failure modes during fatigue cycling with a 10% pre-stretch and a total strain range of $\Delta\varepsilon_t$ = 1.0% or 2.0% at 50Hz frequency. Type 1 failure due to cracks forming along the extrusion pairs and type 2 failure due to strain localization. Based on these failures, they have arrived at a failure criterion corresponding to 1.25 times the change in resistances which is reached after several 10000's of cycles [23].

Sim et al (2013) have proposed a failure map after evaluating the effects of pre-stretch, strain ranges, film thickness and width in fatigue. They have reported that for films under 100nm thickness, intergranular failure is the mode of failure. Films in the range of 200-400nm fail predominantly due to cracks occurring from extrusion and intrusion pairs when subjected to smaller strain amplitudes. At larger strain amplitudes the failure is due to necking and debonding along with the development of cracks from extrusion/ intrusion formations. Higher pre-stretch (strain range) resulted in shorter fatigue life, which they have attributed to increased regions with local necking and debonding. They have concluded that the level of adhesion of the metal film to the substrate, the microstructure of the metal film, thickness range and the strain range, all have an influence on fatigue life of polymer supported thin films [24].

Kokash et al have experimented with porous nano Cu as alternatives to solder in reversed amplitude shear cycling, reporting that the cycles to failure varies with the amplitude to a power of 15, indicating failure due to brittle fracture [25].

A recent paper by Sivasubramony et al. illustrates the behavior of AJP AgNP traces on Upilex in tension and under cyclic tensile loading, including an effect of viscoelastic strain and a systematic dependence of the rate of damage on the initial resistance of the sample and on the strain amplitude. The experiments described in that paper form the basis for experiments presented in this thesis and each of the observed effects have also been described in the chapter on results and discussions [26].

Chapter 3 Experimental Procedure

The test vehicle is as shown in Figure 3.1, is formed on a 2 mil thick DuPont™ Kapton® HN polyimide film or UBE UPILEX®-S 50S polyimide substrate. A single trace of 2 layers of nano silver is aerosol jet printed, by making two passes at the speed of 8mm/s. The ink used, PARU MicroPE®PG-007-AP consisting of Nano silver particles (diameter 20-200nm). It is a water-based ink and is sintered at 200°C for about 40 minutes after printing. The printing is carried out using an Optomec aerosol jet printer. Further details on AJP of AgNP on Upilex can be found in the works of salary et al [27].The samples are printed in batches of 15- 20 on a sheet of polyimide films. These samples are cut to a width of 10mm and length of 120mm using a shear.

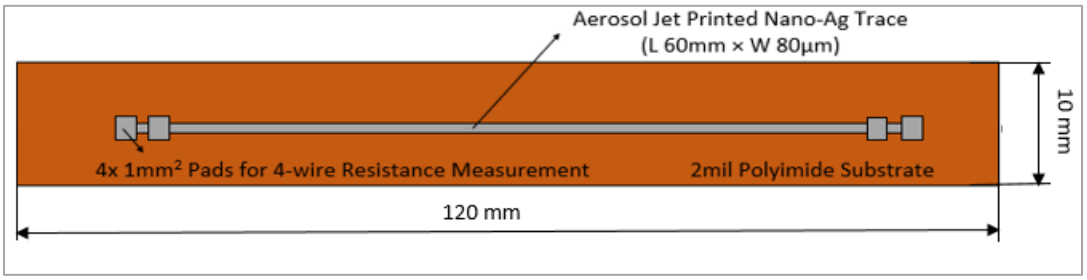

Figure 3.1: Test vehicle- Kapton and Upilex substrates

The surface of the samples and its dimensions are examined using Zeiss Axio Imager M1m optical microscope interfaced to the computer using Axiovision software. Copper leads of length of 35mm and diameter 0.1mm are attached to the four pads shown

in the figure 10 using CircuitWorks CW2400 silver conductive epoxy. The leads are cured at room temperature for 8-12 hours.

The samples along with the leads are tested for tensile loading and tensile fatigue cycling on an Instron 3344, 2000N load cell single column universal tensile testing machine. The samples are clamped at both using aluminum fixtures attached to Instron as shown in Figure 3.2. The aluminum fixture consists of two plates fastened together by allen screws and is attached to the instron column. The Instron can be programmed either using load or extension for test parameters on the computer using Bluehill software at the interface.

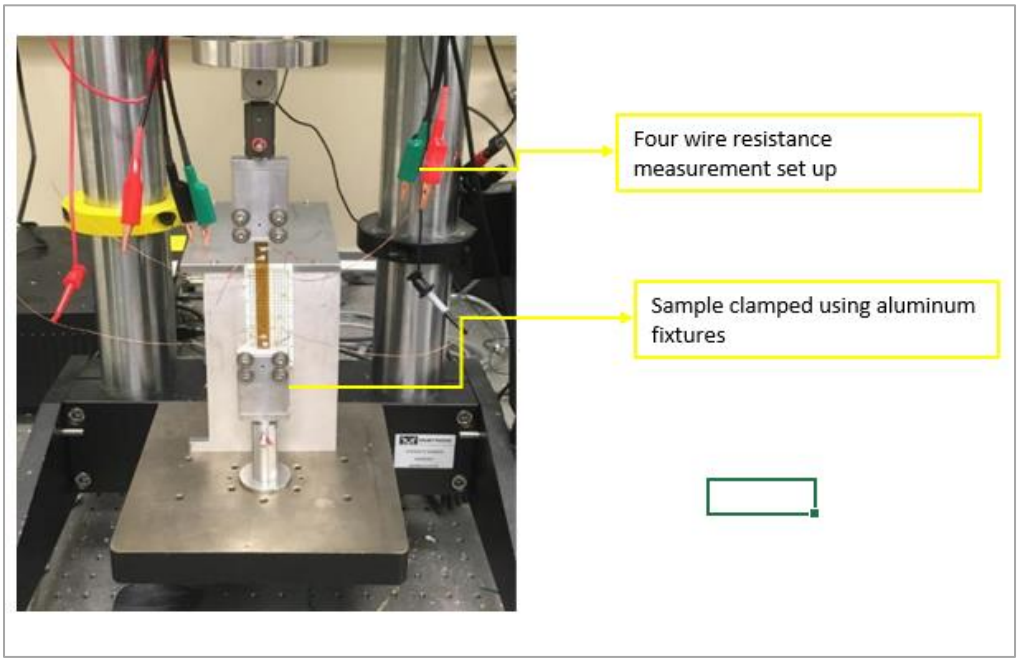

Figure 3.2: Experiment set-up on the Instron

The resistance measurement is carried out in-situ during the tensile testing by Kelvin 4-wire method using a Keithley 2000 series digital multimeter. The 4 wire resistance method eliminates the contact resistances and measured the resistance of the trace within the two inner pads. The multimeter is programmed using KI tool software on

the computer. The resistance values with timestamps are recorded on the computer as .csv files (comma separated values).

To perform tensile tests, the sample is mounted between the two aluminum fixtures. The sample is aligned vertically straight as shown in figure 11 to ensure there's no bending moment and also without any slack. The strain is derived based on the gauge length measured using a Vernier caliper between the edges of the aluminum fixtures. Throughout the thesis we consider only engineering strains. The extent to which the sample is stretched can be set in terms of either displacement or load and the displacement rate for the instron are programmed using the Bluehill software. The digital multimeter and the Instron are set up to run simultaneously at the start of the experiments and the test values are record on the respective computers. The test results are record as a .csv (comma separated values) file which is used for further analysis.

Chapter 4 Result and Discussion

4.1 Comparison of electro-mechanical behavior on the two substrates

4.1.1 Tensile Test

To understand the effect of stretching on the traces, we stretch the aerosol jet printed nano silver trace to a strain of 2% at a nominally constant strain rate of 0.00063 per second using the Instron tensile testing machine. We picked 2% strain because it gives measurable effects that can be repeated. The resistance of the trace is measured in-situ using 4 wire measurement via the digital multimeter. The sample measured an initial resistance of 40.4Ω and we observe that the resistance increases as the sample is stretched (Figure 4.1).

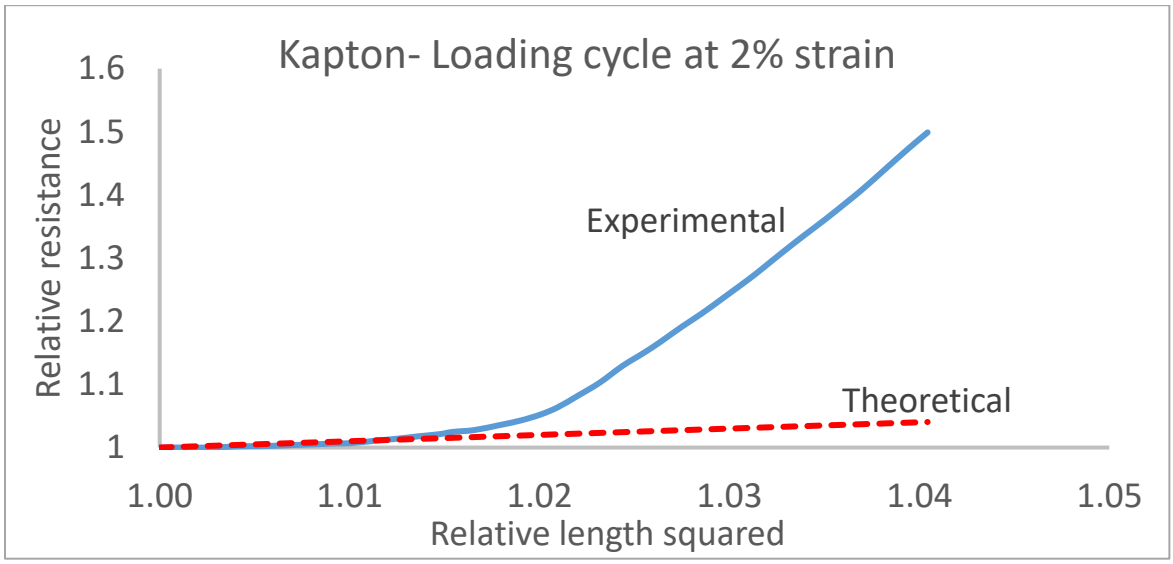

Figure 4.1: Relative resistance vs relative length squared AJP on Kapton

Aerosol jet printed nano silver traces on Kapton behave differently in comparison to electroplated copper on Kapton (Figure 1.1). The resistance of the sample also increases when stretched, but it deviates clearly from the theoretical curve at about 0.5% strain and rapidly increases after 1% strain. One reason aerosol jet printed samples did not behave like electroplated copper samples is that they are porous. Another reason is found to be damage in the form of cracks occurring in the trace when it is being stretched.

The same test was conducted on an aerosol jet printed nano silver trace on an Upilex substrate with an initial resistance of 37.9 Ω. The relative resistance deviates from the square of length behaviour much like for traces on Kapton, Figure 4.2. The relative increase at the peak 2% strain is however about 10% lower for Upilex than for Kapton.

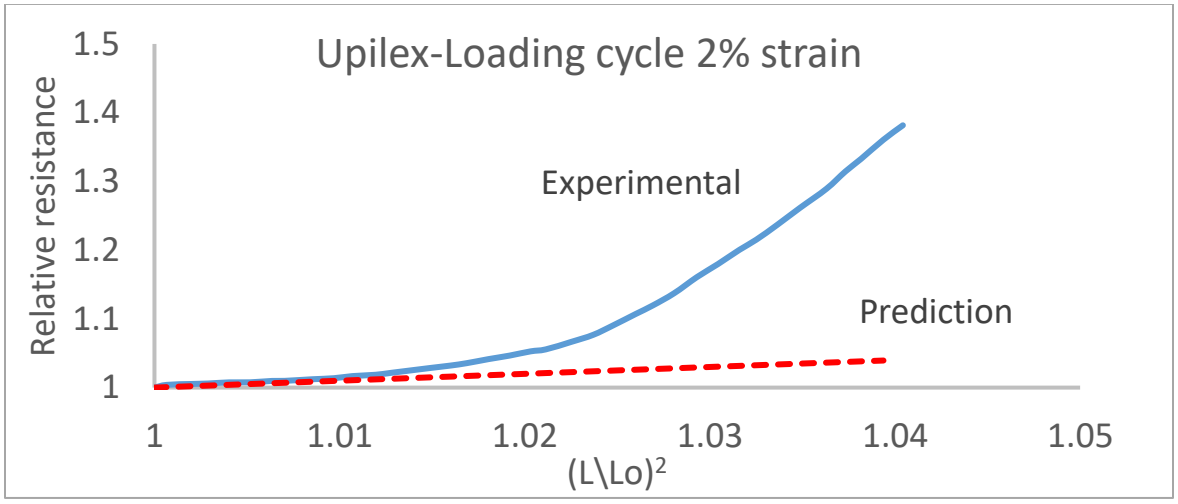

Figure 4.2: Relative resistance vs relative length squared AJP on Upilex

Later in the document, we show that samples starting at a higher initial resistance damage faster in fatigue. To check if differences in the damage rates between Kapton and Upilex was due to the differences in initial resistances, we tested a Kapton and Upilex sample with a lower initial resistances. We see that, in Figure 4.3and Figure 4.4, the magnitude of resistance increase is independent of relative resistance.

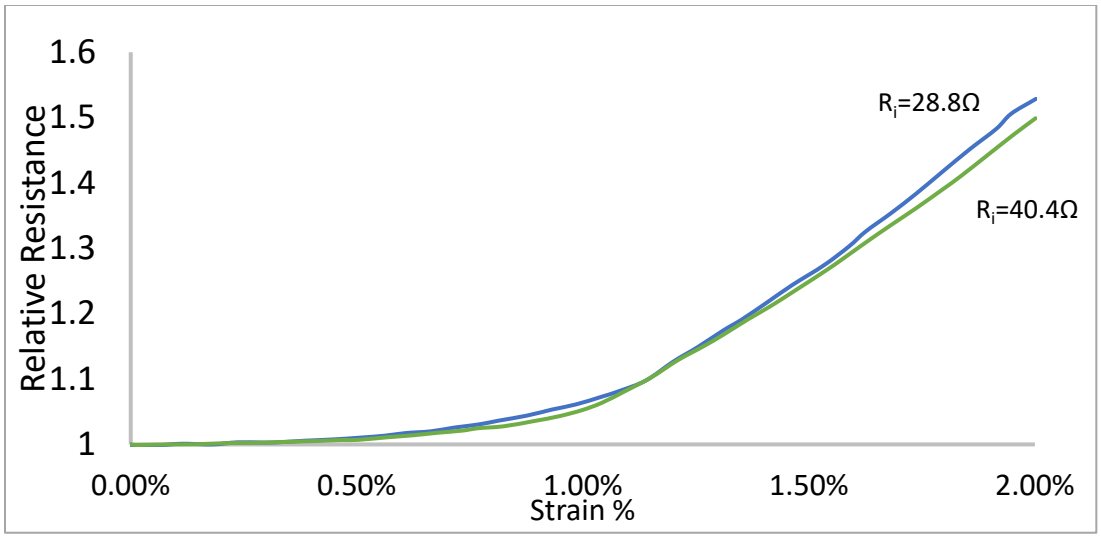

Figure 4.3: Relative resistance of the sample vs. % strain during loading to 2% strain for 2 samples with initial resistances of 28.8 Ω and 40.4Ω on Kapton substrate

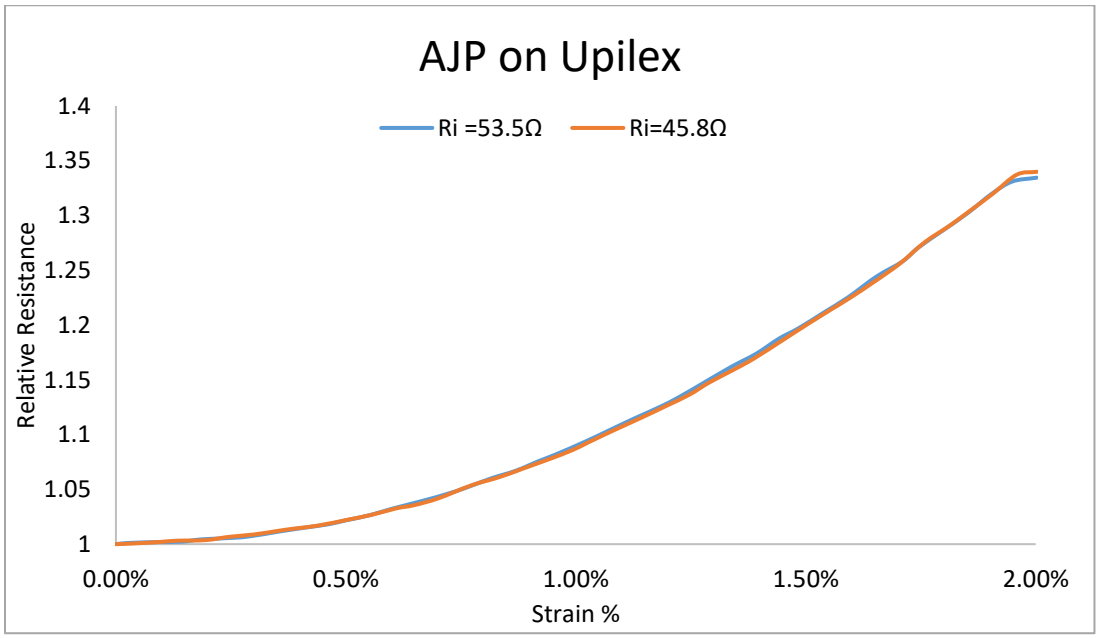

Figure 4.4: Relative resistance of the sample vs. % strain during loading to 2% strain for 2 samples with initial resistances of 45.8 Ω and 53.5Ω on Upilex substrate

We observed that the shape of the curve for change in resistance on both materials looks different. On comparing both the curves (Figure 4.5), we see that at lower nominal strains during the beginning of loading, the change in resistance is much slower than on

Upilex. What it could mean is, deformation on Kapton could be more constrained by trace during the initial part of loading than on Upilex. But, as strain increases Kapton being a more compliant substrate allows for more strain localization and thus damaging faster

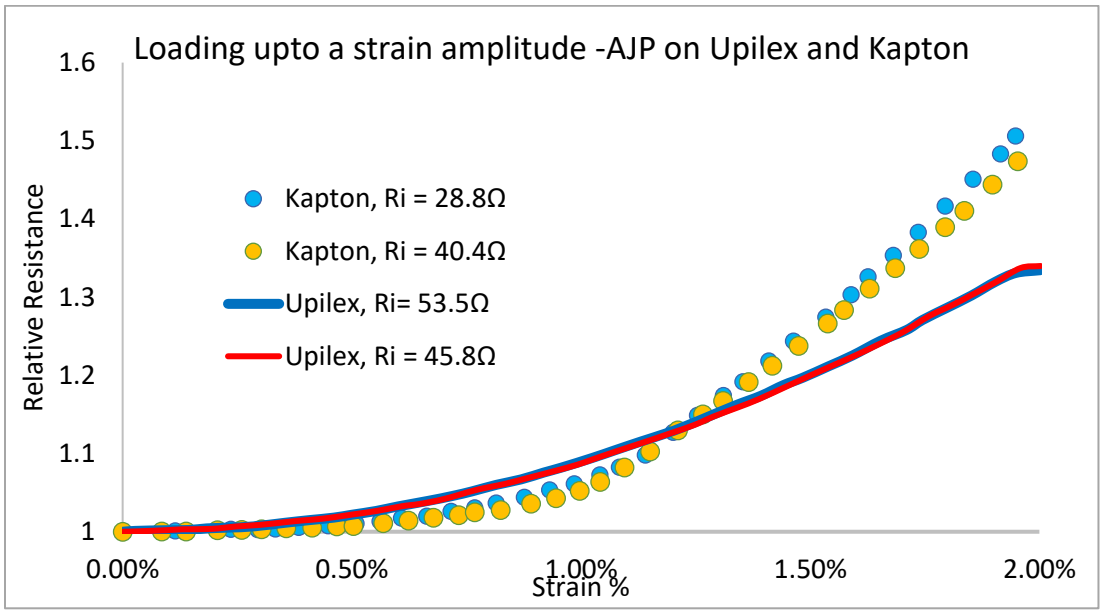

Figure 4.5: Relative resistance of the sample vs. % strain during loading to 2% strain for Upilex and Kapton substrate samples

This behavior is in qualitative agreement to Vlassak's prediction that the crack driving force Z varies linearly with the modulus of the substrates for the present combinations of substrate and trace dimensions [21].

4.1.2 Behavior of traces during unloading

Before we look at the resistance behavior during unloading, we look at the stress (load) vs. strain behavior. Figure 4.6 shows that the sample attains a strain of 2% at a load of 3kgf. During unloading, like for the electroplated Kapton samples above, the Instron reaches 0 load before the cross heads have returned to their initial position. The point at which the load reaches 0 kgf corresponds to around 0.17% strain, which means the sample

is slack and longer than before. As explained, above a part of this deformation is permanent and a part is recoverable over time. The sum of the recoverable strain, called the viscoelastic strain, and the plastic strain for the Kapton substrate is 0.17%.

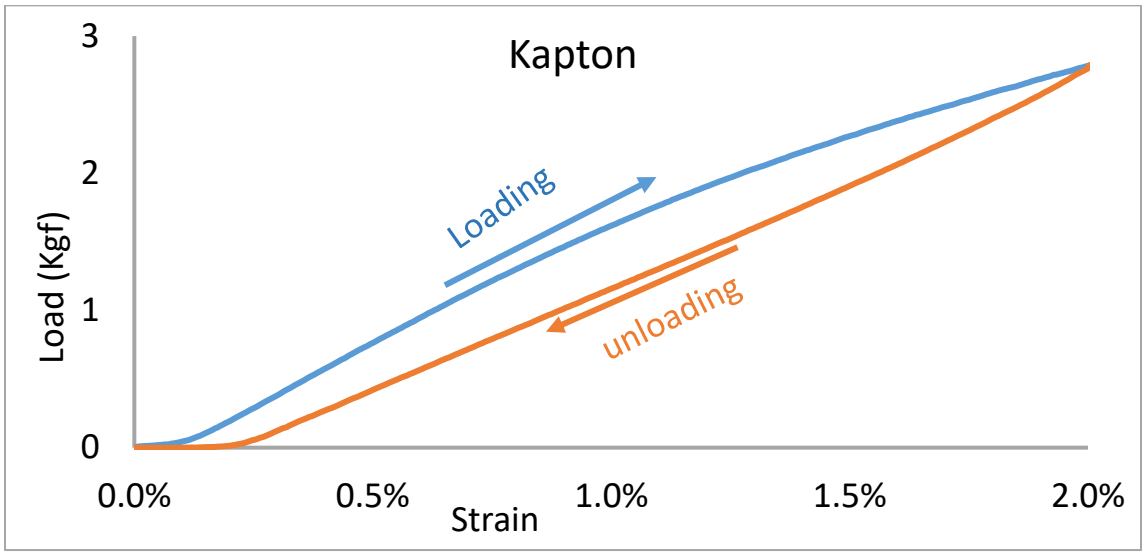

Figure 4.6: Load vs strain for 1 tensile cycle of loading and unloading on Kapton sample

During unloading before reaching zero load the resistance values, unlike for electroplated copper traces, don't trace back the same path as during loading. The relative resistance curve is offset from its loading trajectory, exhibiting a higher resistance at any given strain, Figure 4.7. This increase in resistance can be attributed to the formation of cracks during loading. However, the resistance drops during unloading by more than would be expected if these cracks remained open, an effect that we ascribe to the partial closing of cracks (to make pressure contact or even heal) when the trace contracts. At zero load, when the sample is at the viscoelastic strain of 0.17%, the resistance of the sample is observed to be approximately 10% higher than its initial value (40.4Ω). This means that it is greater than the resistance at a strain of 0.17% during loading. Still, some of the

viscoelastic deformation would recover if the sample was allowed to relax for a longer period, and the resistance would further drop.

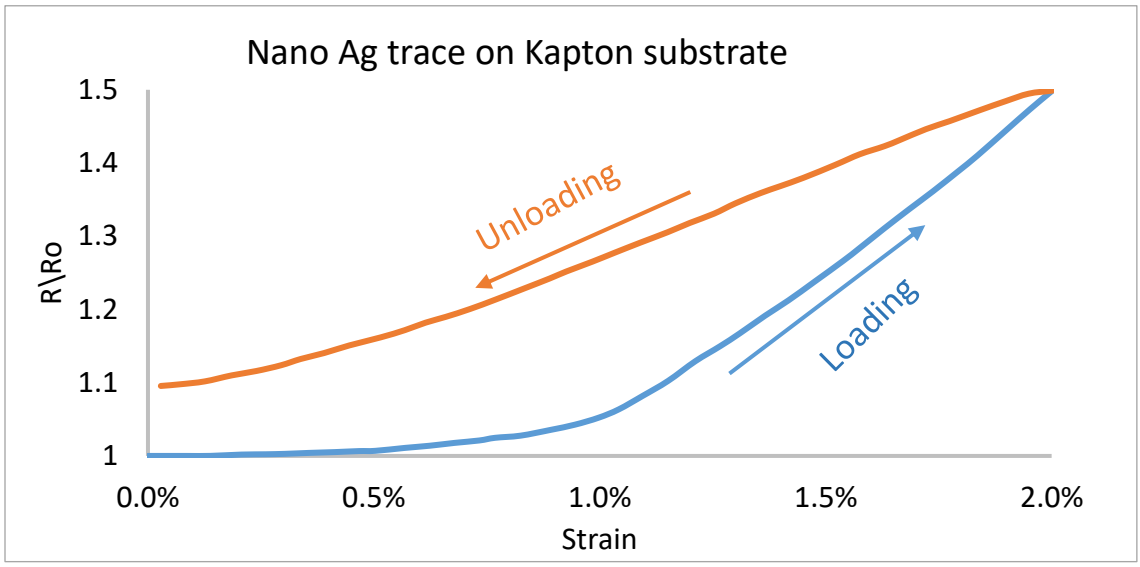

Figure 4.7: Relative resistance vs nominal strain for Kapton sample with initial resistance of 40.4 Ω

Figure 4.8 shows the change in relative resistance for another sample with an initial resistance of 28.8Ω along with the 40.4Ω sample. After unloading, the resistance at the

viscoelastic strain measured around 11% more than the initial resistance.

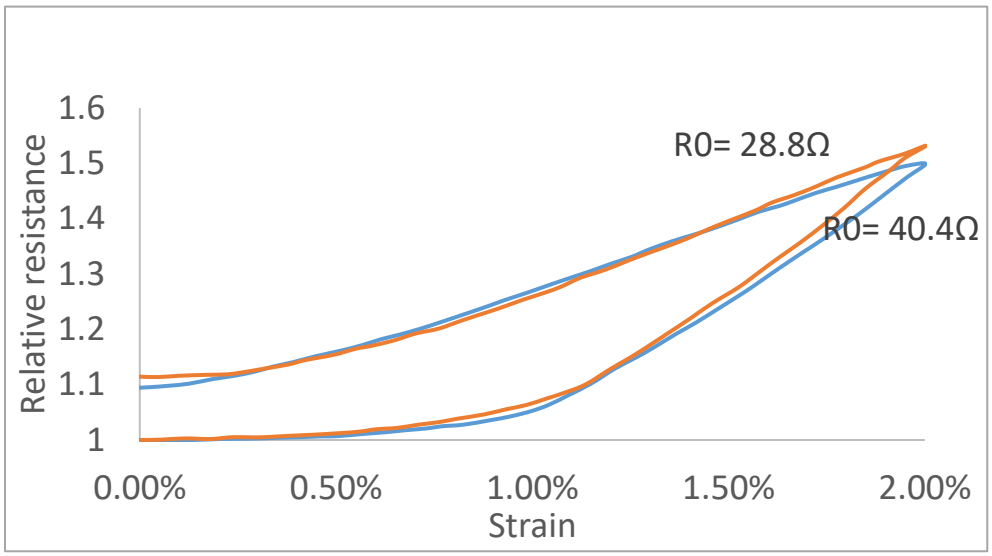

Figure 4.8: Relative resistance vs. nominal strain during loading and unloading for traces on 2 Kapton samples with resistance 40.4 Ω and 28.8 Ω.

Next, we look at the unloading behavior for an AJP nano silver trace on an Upilex substrate sample. The load versus strain data (Figure 4.9) show that the Upilex sample required about 9kgf load, as compared to 3kgf for Kapton, to attain the 2% strain. The viscoelastic strain, after unloading was observed to be around 0.1%, i.e. roughly half that for Kapton.

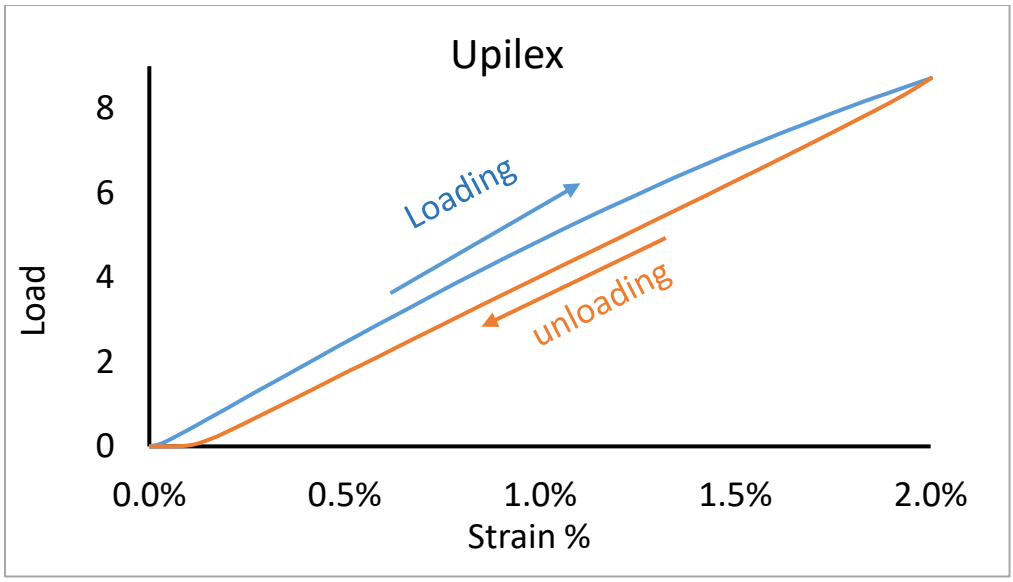

Figure 4.9: Load vs strain for loading and unloading Upilex sample at 2% strain

The initial resistance of the trace was 37.9Ω, and as noted before this increases by about 40% when stretched. Like for Kapton the resistance drops again during unloading, Figure 4.10. The offset in the relative resistance curve during unloading can also here be attributed to crack formation during loading. Also, like on Kapton some of the cracks appear to close again during unloading. At the viscoelastic strain the resistance value is around 10% higher than the initial resistance. This is similar to the value observed on Kapton, even though the resistance at the 2% peak strain was lower and the viscoelastic strain is lower as well.

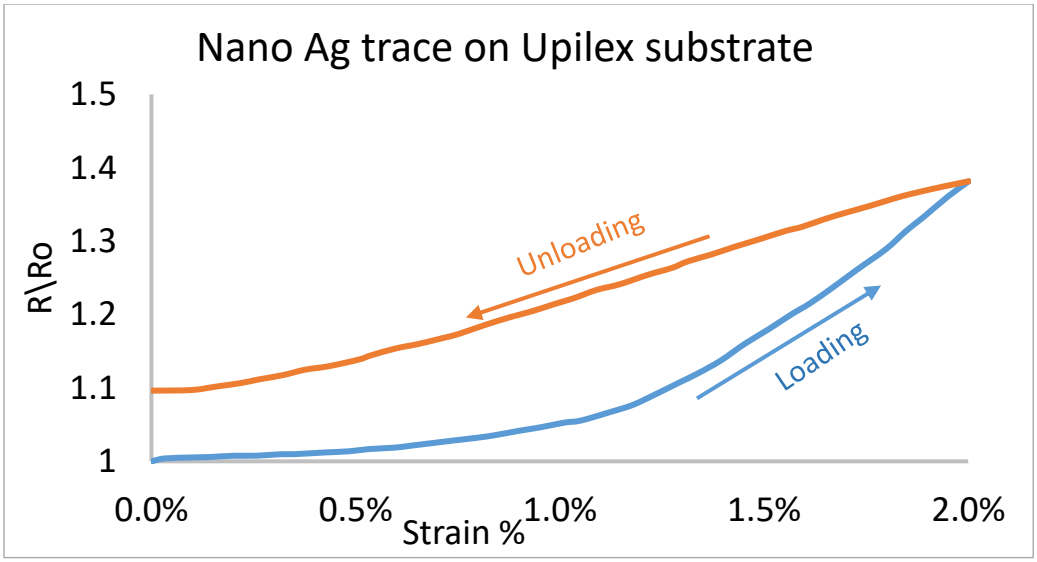

Figure 4.10: Relative resistance vs nominal strain for Upilex sample with initial resistance of 37.9 Ω

Overall, we see that Kapton behaves slightly different compared to Upilex. This is seen to influence the performance of the trace in fatigue (next).

4.1.3 Fatigue performance of the samples

To address this we consider the behavior of the traces on the two substrates when they are stretched multiple times to a fixed amplitude. The resistance of the samples is again measured in-situ using a 4 wire method, while being cycled between a peak strain of 2% and then back to (nominal) 0% for a practical number of cycles at a strain rate of 0.0006 per second. We see the resistance value increase and decrease corresponding to the increase and decrease of strain within each cycle forming a progressively increasing band, Figure 4.11. This gradual increase in resistance at a given strain within each cycle can be attributed to the progression of damage to the trace under the influence of changing mechanical properties of the substrate.

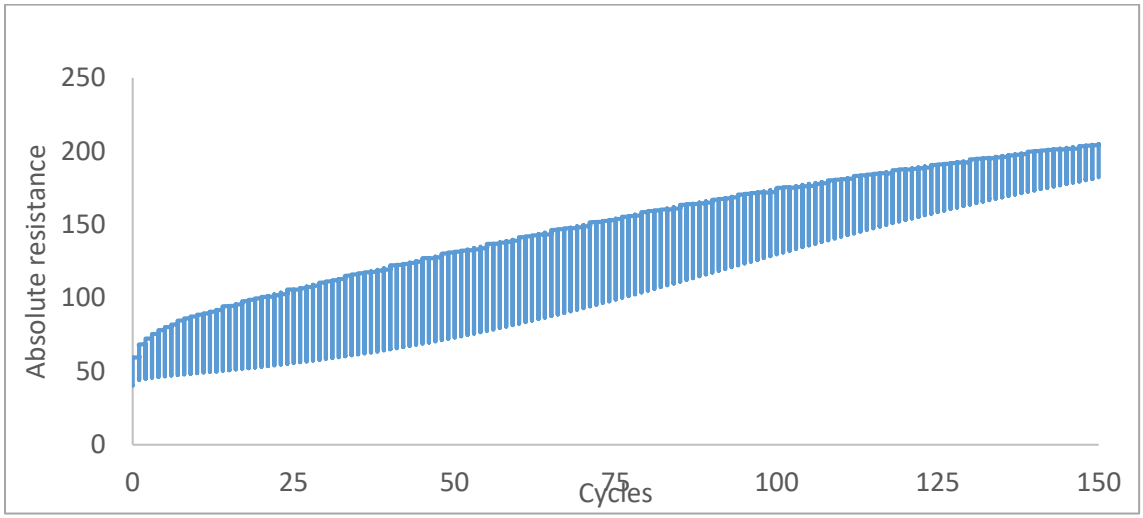

Figure 4.11: Absolute resistance vs. cycles with an strain amplitude of 2% for AJP nano silver trace on Kapton

In order to compare the fatigue performance between substrates or at different strain amplitudes we need to measure the resistance at a particular strain in every cycle. The resistance value at a nominal strain of 0 in every cycle is a combined effect of the viscoelastic behavior and damage to the trace. Hence, measurement at (nominally) zero strain would be misleading, whereas resistance values measured at higher than viscoelastic strain during the loading part of each cycle would serve as a good measure.

4.1.4 Viscoelastic strain of the substrates

The viscoelastic strain on a sample after having been subjected to a higher strain amplitude is more than the viscoelastic strain on a sample after a lower strain amplitude. We quantify the viscoelastic strain (really the sum of the viscoelastic and plastic strain) based on the measurement of the nominal strain at which the load drops to zero. Figure

4.12 shows the evolution of the viscoelastic strain on Kapton and Upilex substrates in cycling to 2% strain amplitude, at a steady strain rate of 0.00063 per second.

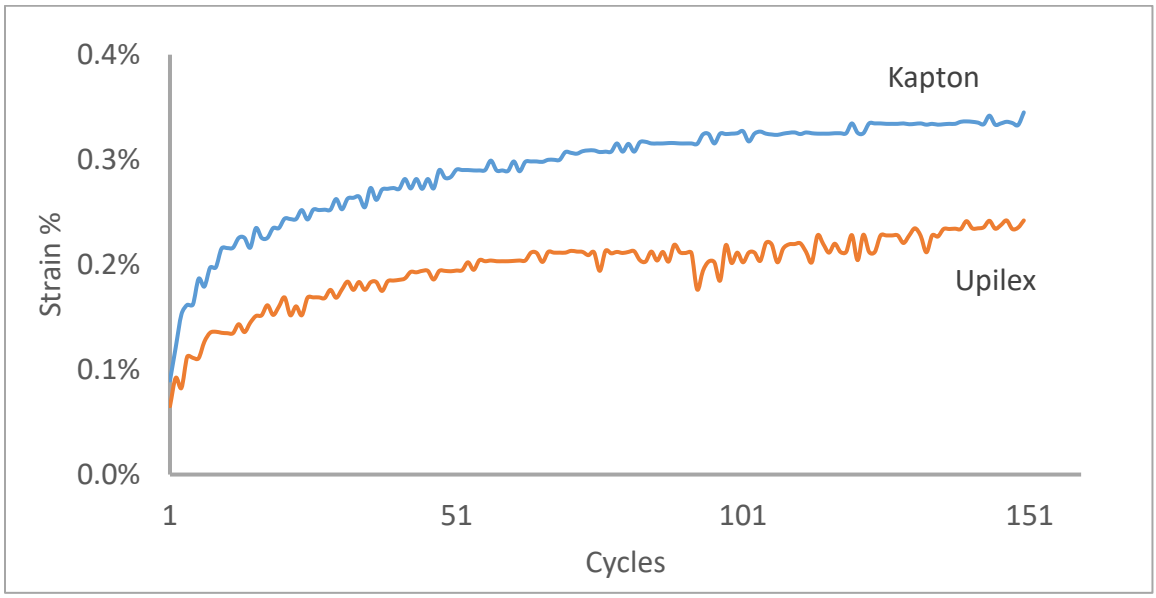

Figure 4.12: Viscoelastic strain values for Kapton and Upilex substrates

The viscoelastic strain is seen to increase and then gradually level off after about 50 cycles for both substrates. Kapton as expected has a higher viscoelastic effect compared to Upilex. After 150 cycles the Kapton substrate has a viscoelastic strain of nearly 0.35% and Upilex about 0.2%.

The resistance values in the present tensile fatigue tests were therefore measured in-situ during the loading part of each cycle at 0.5% strain. Figure 4.13 shows a steady increase in this resistance on Kapton over the number of 2% amplitude cycles.

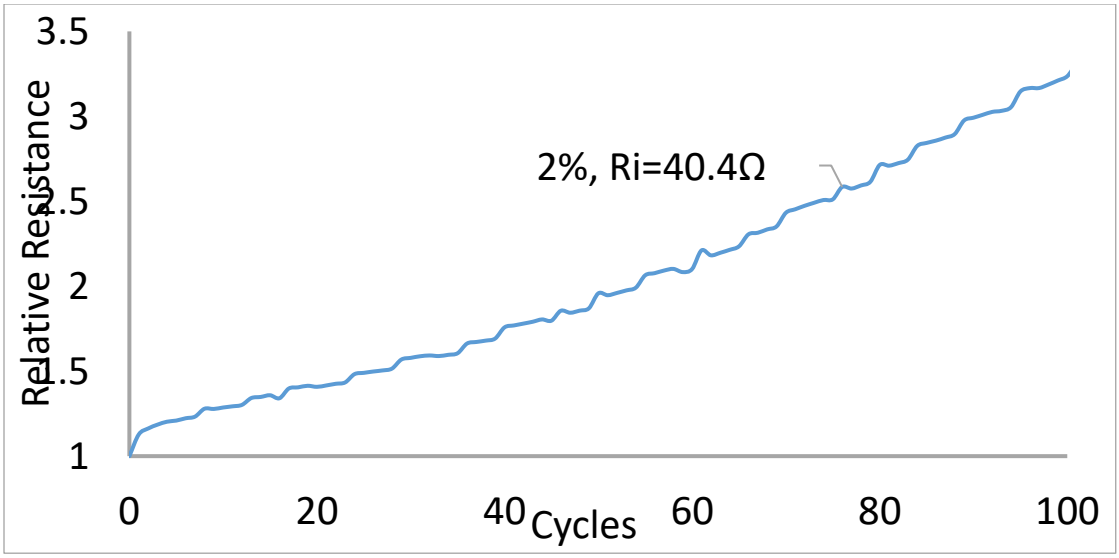

Figure 4.13: Relative resistance at 0.5% strain in each 2% strain amplitude cycle for AJP Ag trace on Kapton

4.1.5 Effect of initial resistance

The initial resistance of the sample depends on many factors such as the width of the trace, porosity, curing time and temperature, age of the samples, etc. In order to ascertain whether differences in initial resistances would correlated with differences in the fatigue performance two AJP Ag traces on Kapton were selected from the same batch having different resistances. These samples were then subjected to fatigue cycling using the Instron machine for 150 cycles at a fixed strain amplitude of 2% and a fixed strain rate of 0.00063 per second. The resistances were measured at 0.5% strain during loading in each cycle. We see, from Figure 4.14, that the resistance increase is almost similar up to 10 cycles but as the number of cycles increases beyond that the sample having the higher initial resistance systematically damages faster than the sample that began with a lower initial resistance. The increase in resistance for samples with initial resistances of 28.9Ω

and 40.4Ω is 200% and 350%, respectively, after 150 cycles at 2% strain amplitude, figure 19. The same phenomenon is true for Upilex samples, Figure 4.15

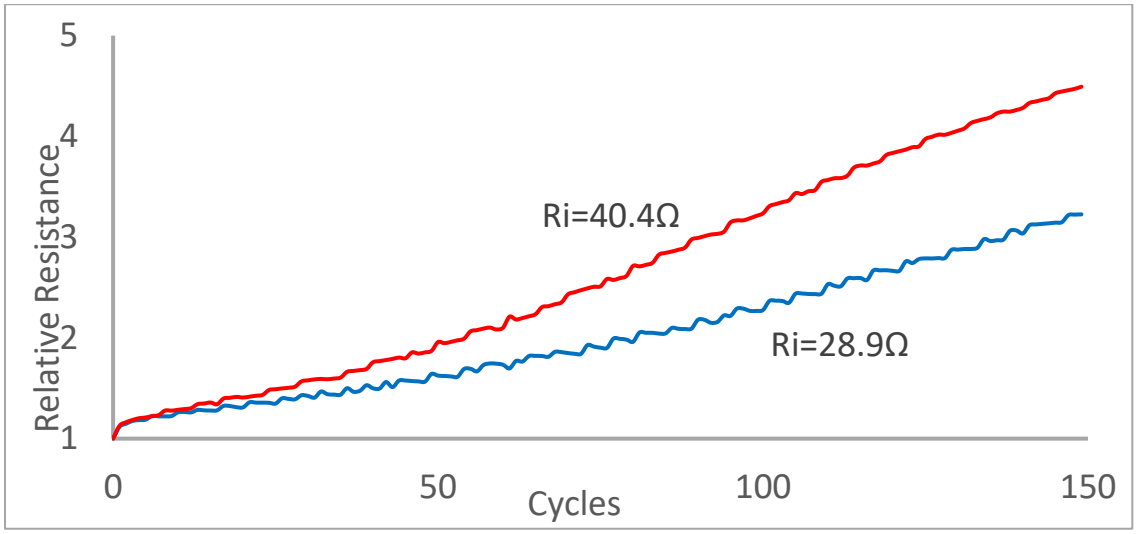

Figure 4.14: Effect of initial resistances on fatigue performance, AJP Ag on Kapton

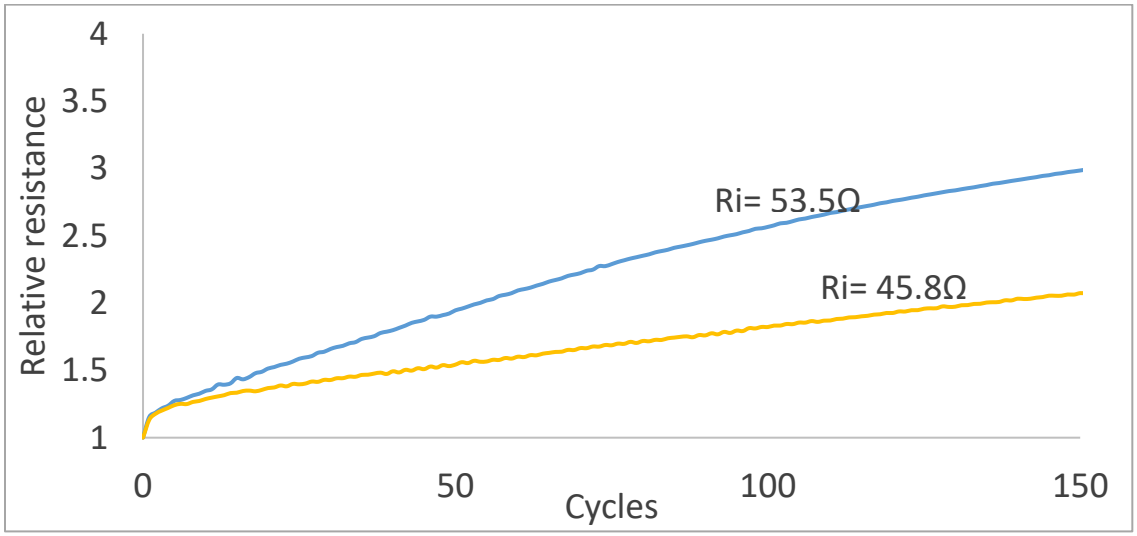

Figure 4.15: Effect of initial resistances on fatigue performance, AJP Ag on Upilex

4.1.6 Damage evolution on Kapton and Upilex substrates

Next, we compared the rate of change in resistance of traces on Kapton and Upilex in cycling to 2% strain amplitude with a strain rate of 0.0006 per second. The traces on

Kapton and Upilex had initial resistances of 40.4Ω and 45.8, respectively. The resistances were again measured at 0.5% strain. Figure 26 shows the rate of change in relative resistance for the trace on the Kapton substrate to be almost twice that of the trace on Upilex, though Upilex sample has a slightly higher initial resistance as compared to Kapton sample. Thus, a major part of the difference in Figure 4.16must be associated with the substrate. As we shall see in a later section it is not an effect of the higher viscoelastic strain remaining in Kapton (in fact, that alone would lead to slower damage).

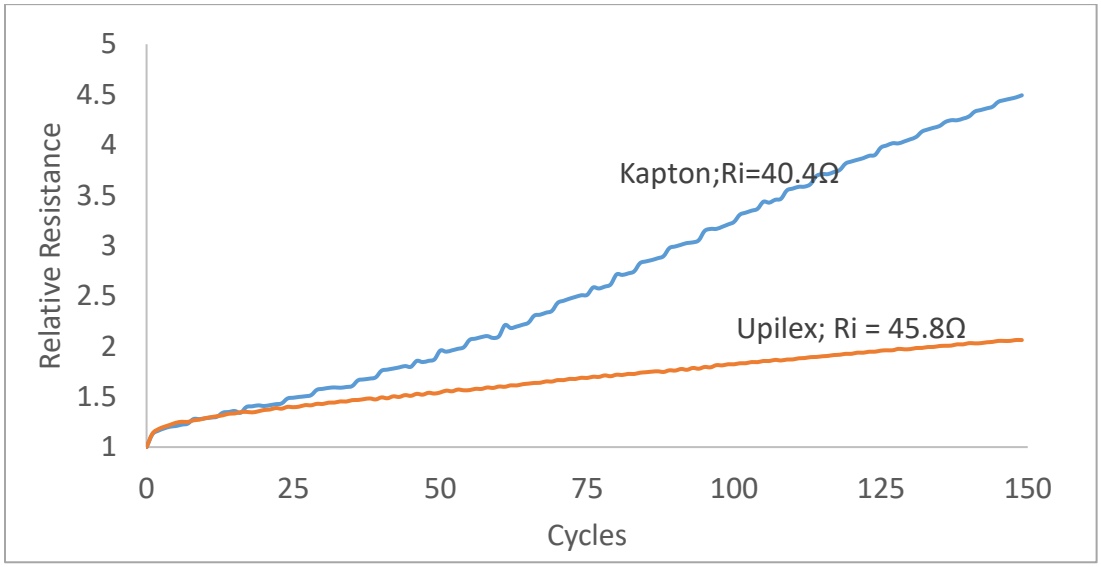

Figure 4.16: Fatigue performance at 2% strain amplitude for trace on Kapton and Upilex substrates

4.1.7 Effect of strain amplitude

Samples with similar initial resistances were cycled in tension at a steady strain rate of 0.0006 per second. The change in resistance was measured in-situ using the 4-wire method in cycling with 1%, 1.5% and 2% strain amplitudes. The resistance values used for comparison were those measured at 0.5% strain. From Figure 4.17, we see that the shape

of the curves for relative resistance vs. cycles is almost the same, but the rate of damage is different. The rate of damage increases with higher strain amplitude.

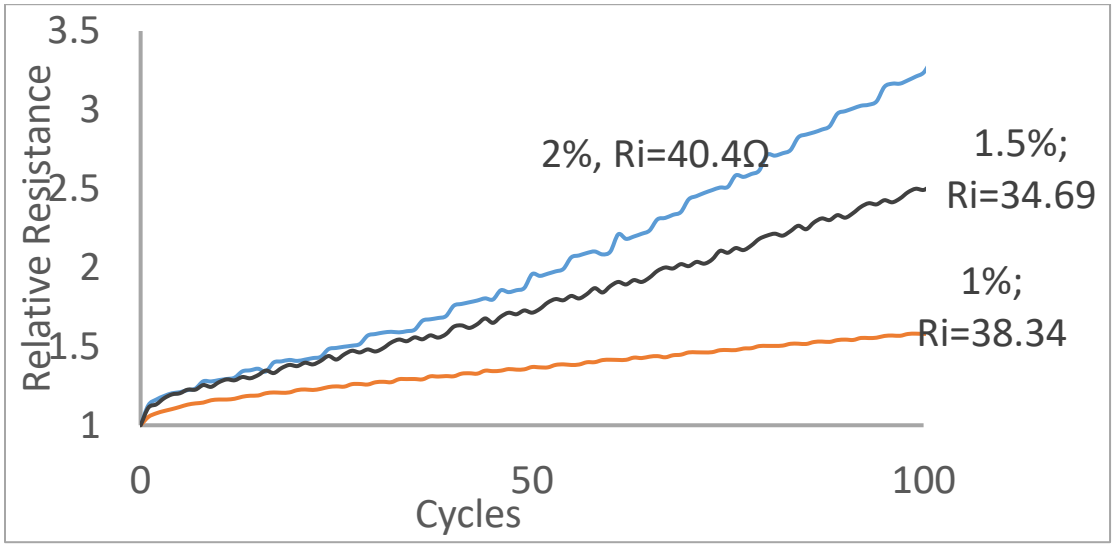

Figure 4.17: Effect of amplitude in fatigue cycling. AJP on Kapton

4.1.8 Scaling

The effect of amplitude on the damage rates was quantified by scaling the curves along the x-axis. Considering the results on Kapton (Figure 4.17) we note that it takes 3.38 times as many cycles to reach a 35% increase in resistance with an amplitude of 1% than with 2%. More generally Figure 4.18 shows how the 1% curve can be scaled onto the 2% curve by dividing the number of cycles by 3.38. Similarly, Figure 4.19 shows how the 1% curve can be scaled onto the 1.5% curve by dividing the number of cycles by 2.75. Both of these figures suggest that the damage evolution may be the same, just differing in terms of the damage rates, up to about twice the initial resistance. Above that there may be differences. The 1.5% curve can be scaled onto the 2% by dividing the number of cycles by 1.23 (Figure 4.20), but the two curves start to diverge above twice the initial resistance. At this point it is not clear whether this is associated with the difference between the actual

initial resistances. Figure 4.14 and Figure 4.15 does suggest not only a lower damage rate for a lower initial resistance, but also less of an upward curvature vs. number of cycles.

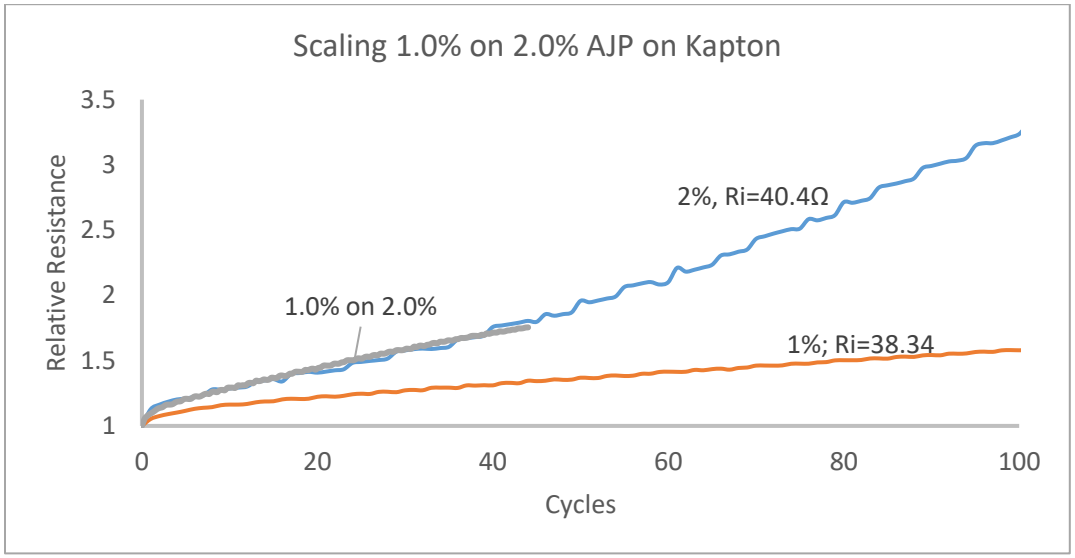

Figure 4.18: Scaling Kapton- damage at 1% strain on 2% strain amplitude

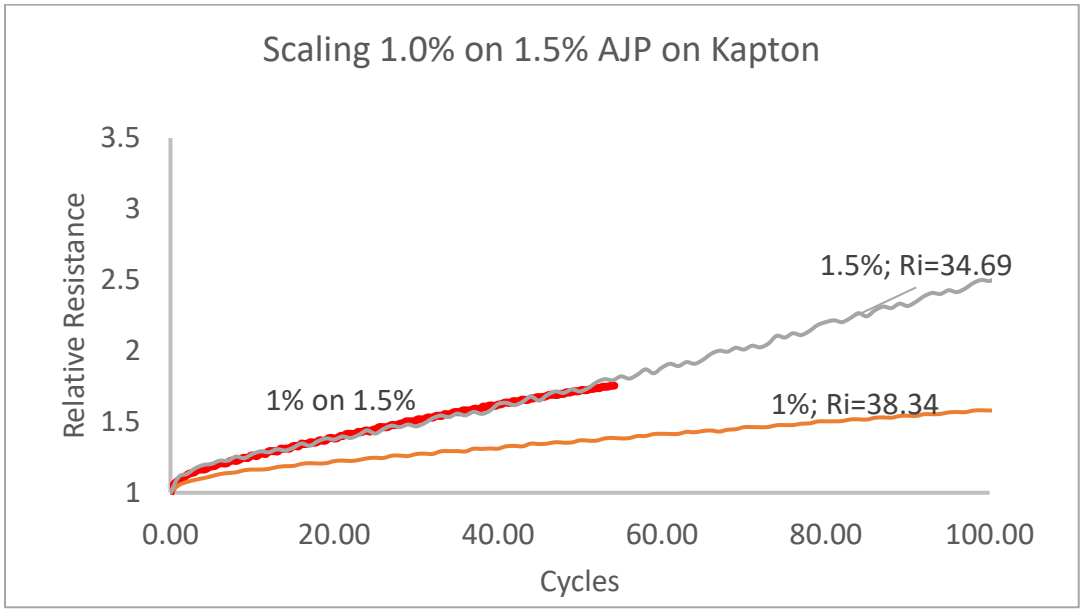

Figure 4.19: Scaling Kapton- damage at 1% strain on 1.5% strain amplitude

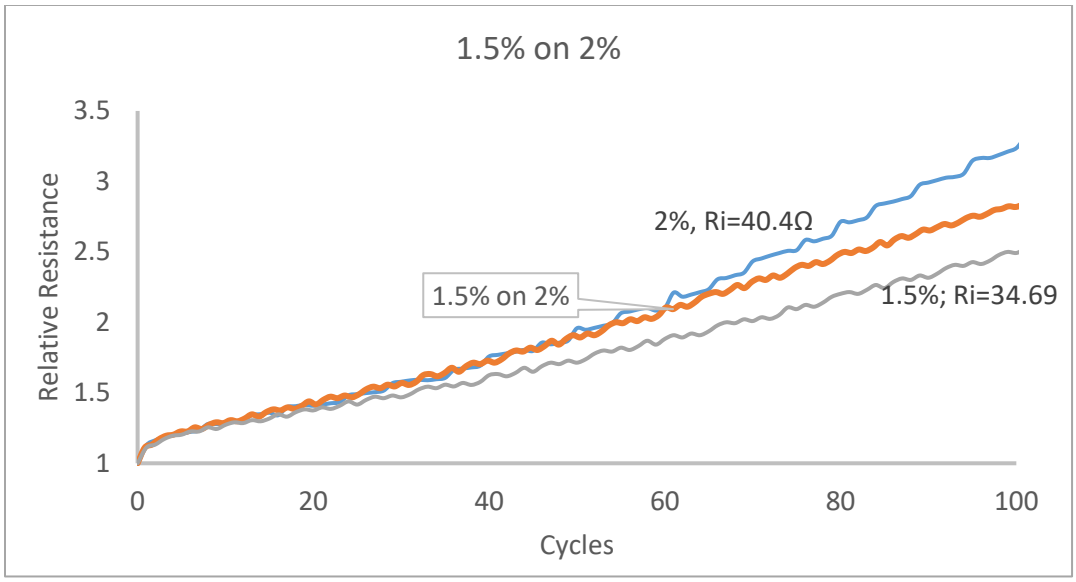

Figure 4.20: Scaling Kapton- damage at 1.5% strain on 2% strain amplitude

We conducted a similar experiment for traces on Upilex, starting with very similar initial resistances and comparing amplitudes of 1%, 1.5% and 2% (Figure 4.21). The scaling factor for 1% on 2%, we see that it takes 11.45 times more cycles to reach a resistance increase of 35% from the initial resistance (Figure 4.22). Figure 4.23, shows that 1% can be scaled on 1.5% by diving the number of cycles by 5.48. In Figure 4.24, 1.5% can be scaled on 2% by diving the number of cycles by 2.09. It is clear that a scaling factors are much greater for Upilex than for traces on Kapton. For example, the 1.5% results could be scaled roughly onto the 2% results by dividing the number of cycles by a factor of 2.09 (Figure 4.24), also much higher than the factor of 1.23 found for Kapton (Figure 4.20). Overall, it is thus clear that the rate of damage increases much faster with amplitude for traces on Upilex than for traces on Kapton. However, the rate was still twice as high on Kapton for an amplitude of 2% (Figure 4.16). Overall, it thus appears that traces on Upilex tend to be damaged slower than traces on Kapton for the same strain amplitude, and more so at lower amplitudes.

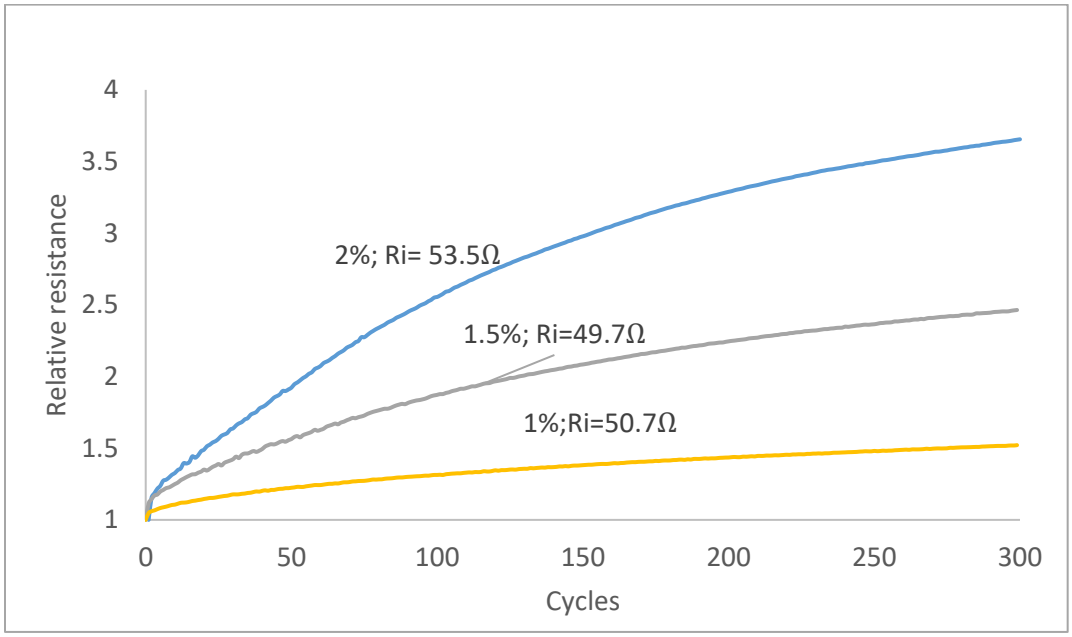

Figure 4.21: Effect of strain amplitude on fatigue. AJP on Upilex

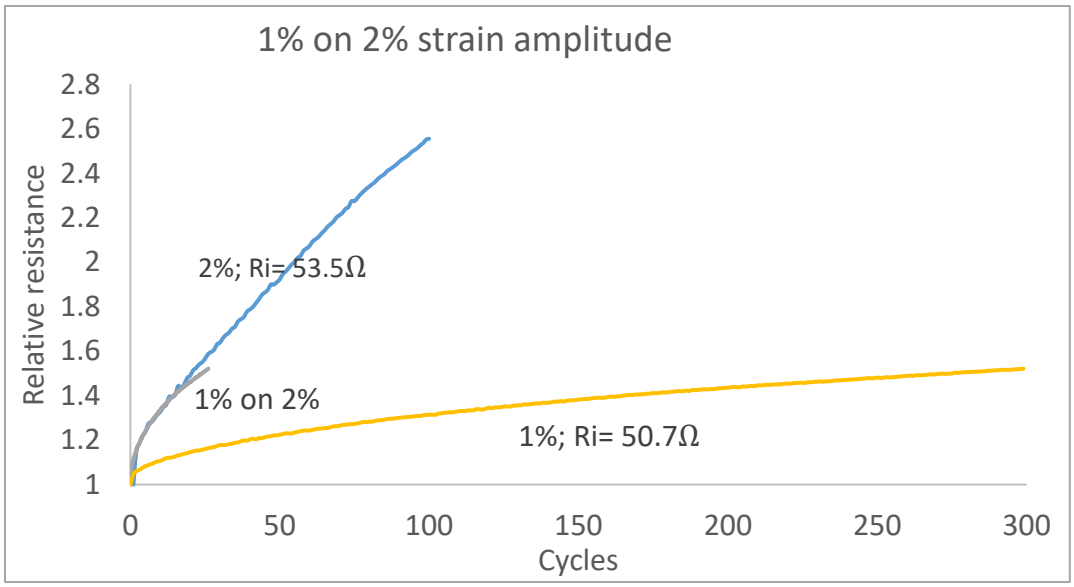

Figure 4.22: Scaling Upilex- damage at 1% strain on 2% strain amplitude

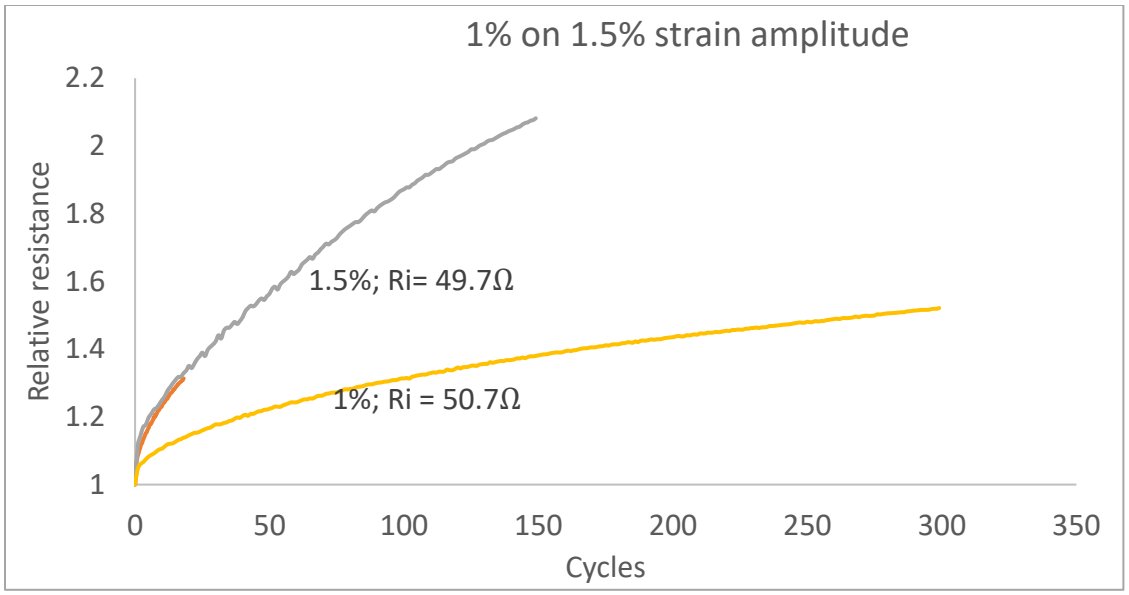

Figure 4.23: Scaling Upilex- damage at 1% strain on 1.5% strain amplitude

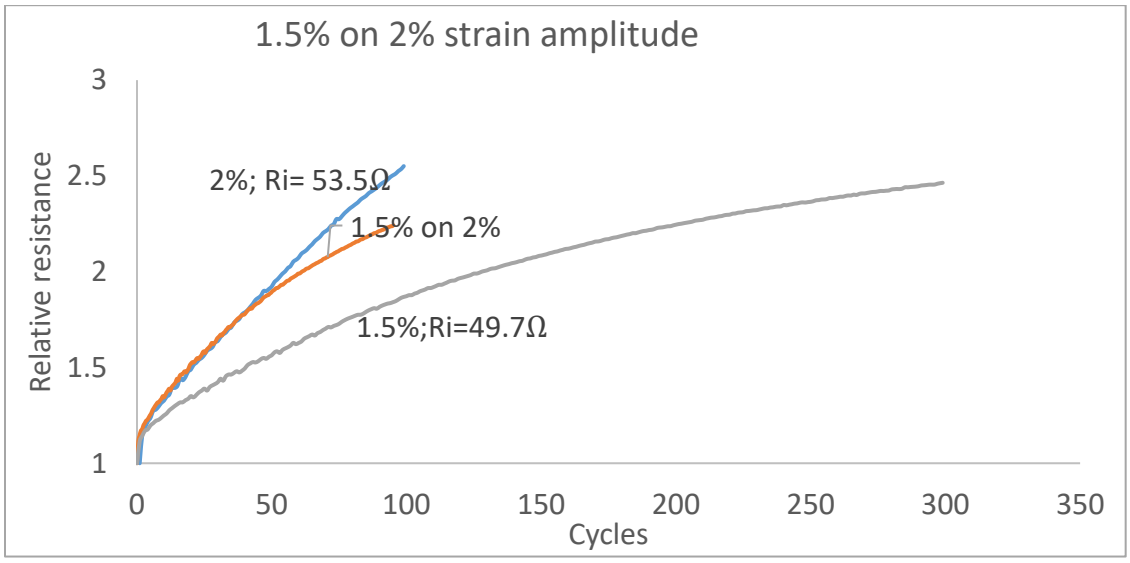

Figure 4.24: Scaling Upilex- damage at 1.5% strain on 2% strain amplitude

The rate of damage for aerosol jet printed nano silver traces is much greater than literature values reported for vapor deposited Ag films of comparable thickness on PET with an acrylic underlayer [23].

4.1.9 Effect of dwell at a strain

The damage to a trace is not expected to be sensitive to the load on the flex, only to the strain. It would thus seem reasonable to assume that the reason traces are damaged more in loading at a lower strain rate is that damage is accumulated over a longer time at any given strain. If so, this would also mean significant damage should accumulate during any dwell at the maximum strain. To assess this we stretched an AJP on Upilex sample to 2% strain at a strain rate of 0.00063 per second and then held it at that strain for 30 minutes. The resistance of the sample was continuously measured using a 4-wire method and after 30 minutes, the sample was unloaded all the way to 0 strain. On analyzing the load data, we notice that the load dropped gradually over time, eventually levelling off, Figure 4.25.

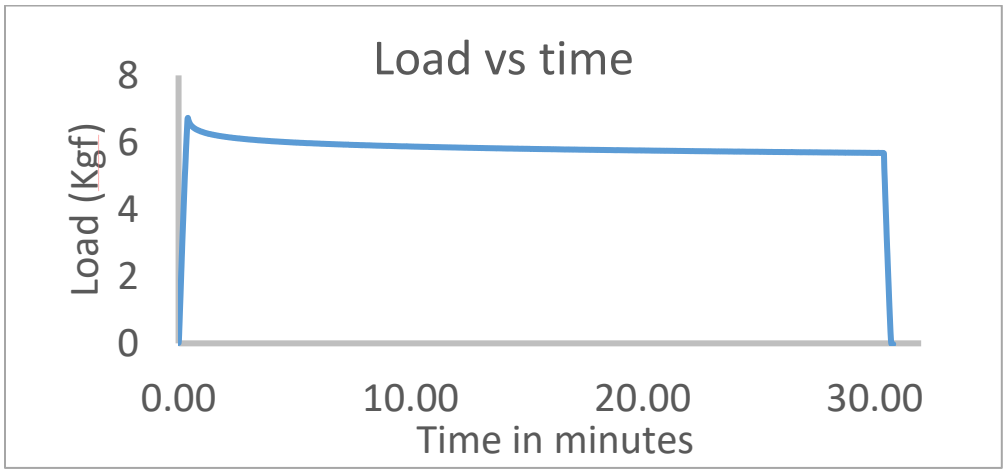

Figure 4.25: Load vs. Time in dwell for Upilex sample at 2% strain

The resistance values on the other hand stayed almost constant, only ending with a 1% increase at the end of the 30 minutes period (Figure 4.26). Also, the resistance dropped to around 12% higher than its initial value during unloading, much the same as without the

dwell. It thus seems that the time at strain may not be the right parameter to explain the observed effects of strain rate.

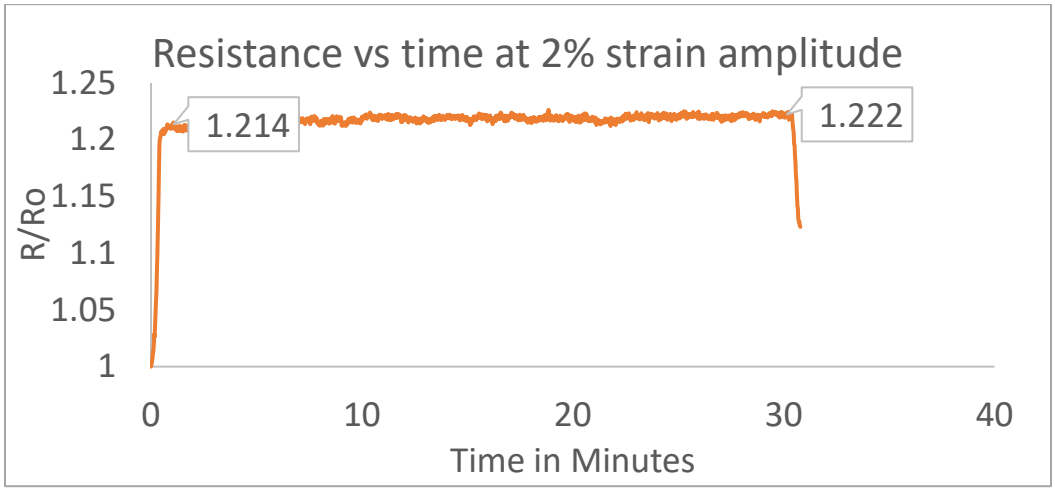

Figure 4.26: Relative resistance vs time in dwell for Upilex sample at 2% strain

We also tested another sample at a higher strain of 5% with a similar set-up. The resistance of this sample increased by about 180% from its initial value when loaded and in this case the resistance value increased by about 4% by the end of the 30 minute dwell, Figure 4.27. During unloading the resistance value then dropped to about 50% higher than its initial value.

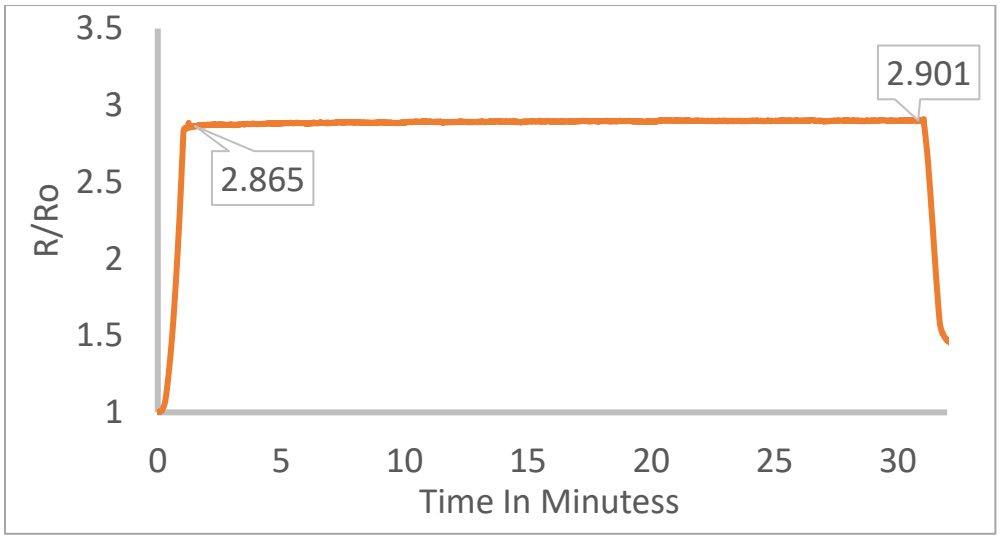

Figure 4.27: Relative resistance vs time in dwell for Upilex sample at 5% strain

4.1.10 Effect of viscoelasticity on resistance of the sample in fatigue

We saw that traces on Kapton systematically damage faster than traces on Upilex substrates and that Kapton has a much higher viscoelastic strain as compared to Upilex. We questioned whether the faster damage of traces on Kapton might be attributed to the higher viscoelastic strains. To check for this we conducted an experiment to compare the rate of damage of Kapton substrate samples cycled between nominal 0 to 2% strain amplitude with a sample cycled at 0.5% to 2% strain amplitude for 150 cycles. We chose the 0.5% strain value because it is higher than the 0.35% viscoelastic strain built up in cycling of Kapton samples with 2% strain amplitude after 150 cycles. The strain rate for the fatigue cycling is 0.00063 per second.

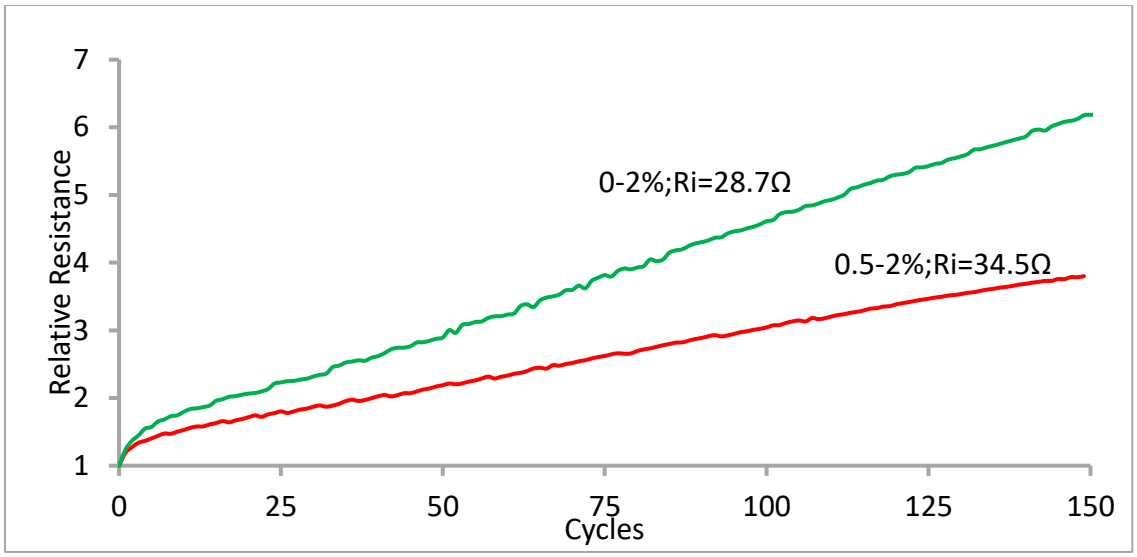

Figure 4.28: Relative resistance vs. cycles at 0.5-2% strain amplitude and 0-2% strain amplitude for Kapton sample

From Figure 4.28, we see that cycling from 0% (nominal) to a strain amplitude of 2% is more damaging than cycling between 0.5% and 2%. This suggests that the faster damage for traces on Kapton substrates is not due to its higher viscoelastic strain.

Based on the results above we don't expect damage accumulated during the 'dwells' at the viscoelastic strains while cycling all the way down to nominal zero strain to be a factor, but just in case we also compared the fatigue performance of traces on Kapton and Upilex samples having similar or close initial resistances in 0.5-2% and 1-2% cycling. The strain rate for the fatigue tests was 0.00063 per second.

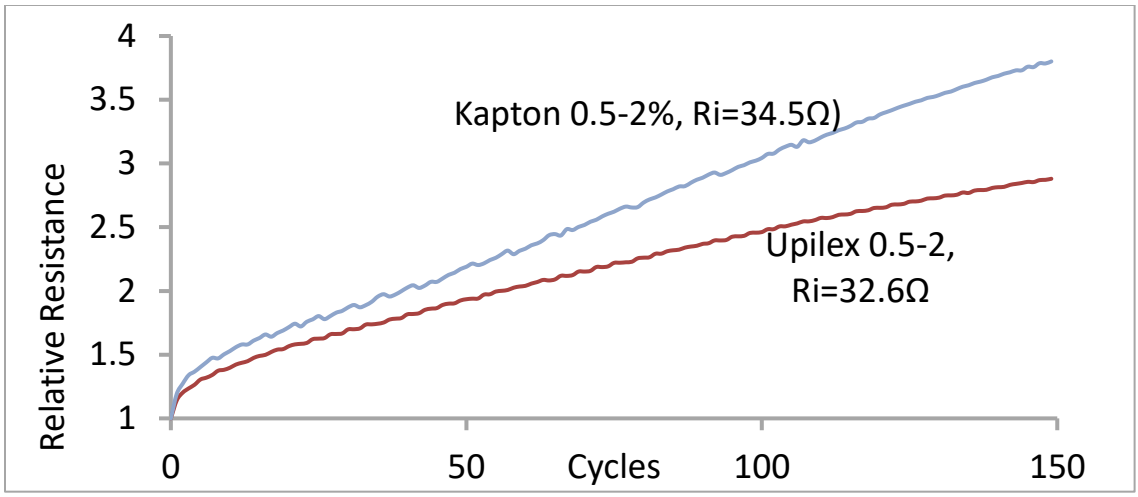

Figure 4.29: Relative resistance vs. cycles for Kapton and Upilex sample at 0.5-2% strain amplitude

Figure 4.29 shows that traces on Kapton still damages faster again than traces on Upilex in fatigue cycling between 0.5% and 2% strain. In either case the rate of damage is less than in 0 (nominal) -2% cycling. The same trend continues in 1-2% cycling (Figure 4.30).

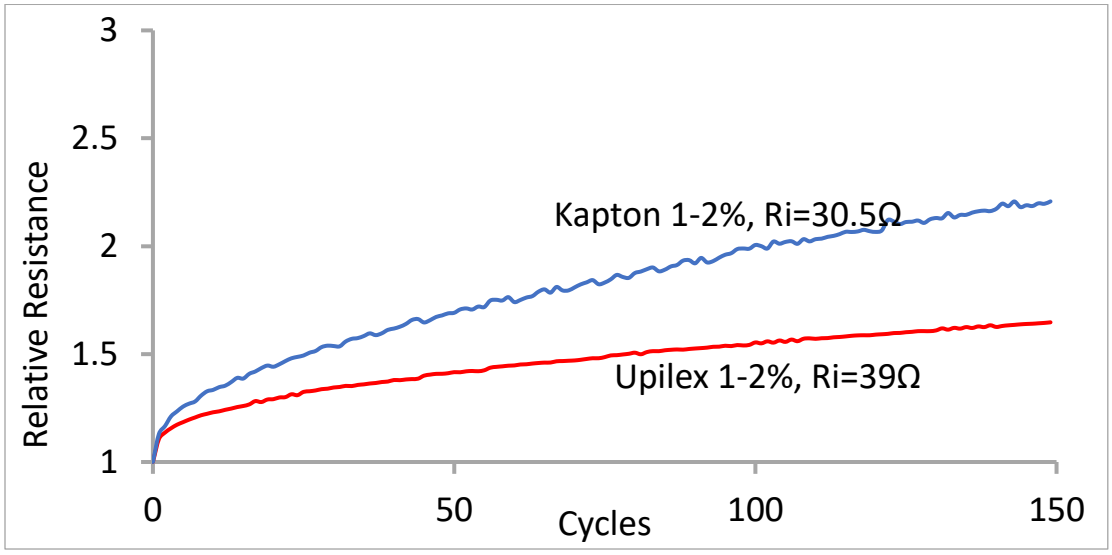

Figure 4.30: Relative resistance vs. cycles for Kapton and Upilex at 1-2%strain amplitude

In conclusion, traces damage faster on Kapton than on Upilex for reasons that do not have anything to do with the difference in viscoelastic strain. Instead, we suggest that the lower stiffness of Kapton allows for slightly more strain localization. An alternative would be if the adhesion to Kapton is lower, allowing for easier (local) interfacial debonding. As discussed in the literature section Li et al. [17] showed the rupture strain for ductile metal films on elastomer substrates to increase rapidly when the substrate modulus increased from 100MPa to 150MPa, but it is not clear whether the same trend remains significant for nano-porous Ag at moduli above 2.5GPa (modulus of Kapton). However, we suggest that effects on fatigue rates may be stronger than effects on rupture strain. Anyway, fatigue failure surfaces of the present traces are shown to be microscopically brittle, so a more appropriate discussion may that of Suo et al. [15] for brittle films (albeit non-porous) on polymer substrates. They argue that the substrate constrains the opening of the initial crack and offer an expression for the driving force for steady state crack growth that varies with ratio of the elastic moduli of the film and the substrate.

Chapter 5 Conclusion

Stretching a trace leads to increased resistance due to (a) increase in length and reduction in cross section, and (b) possibly due to damage. Electroplated copper on Kapton can be stretched to more than 35-50% without significant damage when adhered to a polymer substrate that prevents strain localization. But in the case of the AJP AgNP traces on a polymer substrate, the damage is greater in magnitude in comparison with electroplated Cu traces on Kapton or electron beam deposited Ag traces on PET [18]. The traces damage lot faster in terms of change in resistance by stretching only to 0.5-1% strain. This increase in resistance is greater than explainable based on length and cross section alone. We suggest that thus could be due to formation of distributed micro cracks near the interface to the substrate, i.e. cracks that have to grow a lot before they become visible by SEM.

On stretching traces on Kapton, the deformation of the substrate is slightly more constrained by the trace when stretched to same nominal strain, leading to less resistance increase at beginning of loading. At higher strain, Kapton being more compliant than Upilex also allows for slightly more strain localization and thus faster damage there. This behavior is in qualitative agreement with predications made by Vlassak [21], indicating linear variation of the crack driving force with substrate modulus for the present combinations of substrate and trace dimensions and properties.

The resistance drops again during unloading, but the resistance is greater than resistance observed at the same strain during loading. The resistance drop during unloading, however is less than if the cracks stayed open, which could be attributed to the cracks partially closing or healing. The remaining resistance increase after unloading completely is due to viscoelastic strain on the substrate keeping the trace stretched somewhat. We also see that Kapton, having a much lower tensile modulus than Upilex, is much more compliant, and ends up having greater viscoelastic strain.

The rate of resistance increase of the samples seems insensitive to initial resistances when first stretched, however this is not the case during fatigue. The rate of damage observed during fatigue was greater for samples with higher initial resistances, shifting the dependence of fatigue performance on the quality of the traces. The rate of damage in cycling is greater for traces on Kapton than on Upilex for amplitudes of 2% or less. In either case the rate is much greater than literature values for vapor deposited Ag films of comparable thickness on PET [24].

The rate of damage is also found to increase with increase in strain amplitude for both cases. However, the variation of damage with amplitude (or strain range) for the traces on Kapton and Upilex substrates is not the same. The damage increases faster with amplitude on Upilex than on Kapton, overall leading to life of less than 10,000 cycles for both as compared to literature values [22]. The cycling induced cracking is brittle, observed by Sivasubramony et al[26], but the sensitivity to amplitude is much weaker than for self-supporting brittle materials. The number of cycles to failure versus amplitude is not a power dependence so the Coffin-Manson relationship does not apply[25].

In general, traces on Kapton damage faster than on Upilex in fatigue, and the difference is not a result of the higher viscoelastic strain for Kapton. On the contrary, damage progresses very slowly at a fixed strain, and cycling to the same amplitude from a minimum strain higher than the viscoelastic leads to slower damage. It could be possibly due to other factors as described in literature[21][24], due to strength of interfacial adhesion of traces with the substrate or due to lower stiffness of Kapton. The observed effects overall could be regarded as a step towards assessing the behavior of AJP AgNP traces on PI substrates.

Chapter 6 Future work

Aerosol jet printing is a relatively new technology. Long term reliability of these traces can only be understood through extensive experiments and modelling based on service conditions. We have only attempted to understand the electro-mechanical behavior of AJP AgNP traces on two polyimide substrates based on tensile and cyclic loading. Generalized modelling for practical applications may necessitate experiments that extended to:

1) Determining the strength of interfacial bonding between the trace and the substrate, and its effects in fatigue

2) The effect of substrates stiffness could be investigated further with respect to AJP traces, considering the fact that the traces are less ductile as compared to electroplated traces.

3) Understanding damage caused to the trace due to cycling at varying combination of strain amplitudes. In realistic service conditions, the strains experienced by interconnects mostly would alternate between a higher strain and a lower strain for short intervals of time.

4) Other mechanical aspects of testing such performance during cyclic bending, combinations of tensile and compressive bending, and twisting.

5) Study the effect of strain rate at varying strain amplitudes. Initial experiments have indicated higher damage at lower strain rates. Assessing the fatigue behavior in low strain amplitudes for cycles in order of 10,000's could lead to some interesting insights.

6) Effects of external environment on the traces. Fluctuations in operating temperatures and humidity may affect the chemical and electrical properties of the traces. Accelerated aging tests such as annealing at higher temperature's for durations of time periods, thermal cycling between lower and higher temperatures, and exposure to increased humidity. This experiments would lead us to better understand the underlying mechanisms in using AgNP for electrical traces.

7) To protect from the external elements, the traces most likely would be laminated or encapsulated. The material properties of the encapsulant and its geometry could be an influence on the reliability of the trace.

Chapter 7 References

[1] D. E. Leber, B. N. Meek, S. D. Leija, D. G. Wilson, R. L. Chaney, and D. R. Hackler, "Electromechanical Reliability Testing of Flexible Hybrid Electronics Incorporating FleX Silicon-on-Polymer ICs," IEEE WMED Conf. Proc., p. 38~41, 2016.

[2] R. R. Keller, J. M. Phelps, and D. T. Read, "Tensile and fracture behavior of free-standing copper films," Mater. Sci. Eng. a-Structural Mater. Prop. Microstruct. Process., vol. 214, no. 1–2, pp. 42–52, 1996.

[3] N. Lu, X. Wang, Z. Suo, and J. Vlassak, "Metal films on polymer substrates stretched beyond 50%," Appl. Phys. Lett., vol. 91, no. 22, pp. 1–4, 2007.

[4] "Rotogravure Print Process | Gravure Printed Flexible Packaging Specialists | Discovery Flexibles." [Online]. Available: http://www.discoveryflexibles.com/rotogravure/. [Accessed: 22-Jul-2018].

[5] M. Pudas, N. Halonen, P. Granat, and J. Vähäkangas, "Gravure printing of conductive particulate polymer inks on flexible substrates," Prog. Org. Coatings, vol. 54, no. 4, pp. 310–316, 2005.

[6] M. Keener, "Printing Techniques for Electronics."

[7] Das Raghu, "Printing Technologies find their Place in Printed Electronics | IDTechEx Research Article," 2017. [Online]. Available: https://www.idtechex.com/research/articles/printing-technologies-find-their-place-in-printed-electronics-00010920.asp. [Accessed: 22-Jul-2018].

[8] J. Li, F. Rossignol, and J. Macdonald, “Inkjet printing for biosensor fabrication: Combining chemistry and technology for advanced manufacturing,” Lab Chip, vol. 15, no. 12, p. 2544, 2015.

[9] C. Goth, S. Putzo, and J. Franke, “Aerosol Jet printing on rapid prototyping materials for fine pitch electronic applications,” Proc. - Electron. Components Technol. Conf., pp. 1211–1216, 2011.

[10] V. R. Marinov et al., “Direct-write vapor sensors on FR4 plastic substrates,” IEEE Sens. J., vol. 7, no. 6, pp. 937–944, 2007.

[11] M. Maiwald, C. Werner, V. Zoellmer, and M. Busse, “INKtelligent printed strain gauges,” Sensors Actuators, A Phys., vol. 162, no. 2, pp. 198–201, 2010.

[12] C. S. Jones, X. Lu, M. Renn, M. Stroder, and W. S. Shih, “Aerosol-jet-printed, high-speed, flexible thin-film transistor made using single-walled carbon nanotube solution,” Microelectron. Eng., vol. 87, no. 3, pp. 434–437, 2010.

[13] B. Clifford, D. Beynon, C. Phillips, and D. Deganello, “Printed-Sensor-on-Chip devices – Aerosol jet deposition of thin film relative humidity sensors onto packaged integrated circuits,” Sensors Actuators, B Chem., vol. 255, pp. 1031–1038, 2018.

[14] “AEROSOL JET PRINTED ANTENNA For Consumer Electronics and Industrial Applications,” 2017. [Online]. Available: http://www.optomec.com. [Accessed: 22-Jul-2018].

[15] Z. Suo, J. Vlassak, and S. Wagner, “MICROMECHANICS OF MACROELECTRONICS,” vol. 3, no. 6, pp. 321–328, 2005.

[16] Y. Xiang, T. Li, Z. Suo, and J. J. Vlassak, “High ductility of a metal film adherent on a polymer substrate,” Appl. Phys. Lett., vol. 87, no. 16, pp. 1–3, 2005.

[17] T. Li, Z. Huang, Z. Suo, S. P. Lacour, and S. Wagner, “Stretchability of thin metal films on elastomer substrates,” Appl. Phys. Lett., vol. 85, no. 16, pp. 3435–3437, 2004.

[18] G. D. Sim, S. Won, C. Y. Jin, I. Park, S. B. Lee, and J. J. Vlassak, “Improving the stretchability of as-deposited Ag coatings on poly-ethylene-terephthalate substrates through use of an acrylic primer,” J. Appl. Phys., vol. 109, no. 7, 2011.

[19] H. Mei, Y. Pang, and R. Huang, “Influence of interfacial delamination on channel cracking of elastic thin films,” Int. J. Fract., vol. 148, no. 4, pp. 331–342, 2007.

[20] Z. Suo and J. W. Hutchinson, “Steady-state cracking in brittle substrates beneath adherent films,” Int. J. Solids Struct., vol. 25, no. 11, pp. 1337–1353, 1989.

[21] J. J. Vlassak, “Channel cracking in thin films on substrates of finite thickness,” Int. J. Fract., vol. 119/120, no. 1979, pp. 299–323, 2003.

[22] G. D. Sim, S. Won, and S. B. Lee, “Tensile and fatigue behaviors of printed Ag thin films on flexible substrates,” Appl. Phys. Lett., vol. 101, no. 19, 2012.

[23] G. D. Sim, Y. Hwangbo, H. H. Kim, S. B. Lee, and J. J. Vlassak, “Fatigue of polymer-supported Ag thin films,” Scr. Mater., vol. 66, no. 11, pp. 915–918, 2012.

[24] G. D. Sim, Y. S. Lee, S. B. Lee, and J. J. Vlassak, “Effects of stretching and cycling on the fatigue behavior of polymer-supported Ag thin films,” Mater. Sci. Eng. A, vol. 575, pp. 86–93, 2013.

[25] M. Z. Kokash et al., “Assessing the Reliability of High Temperature Solder Alternatives,” 2017 IEEE 67th Electron. Components Technol. Conf., pp. 1987–1995, 2017.

[26] R. S. Sivasubramony et al., “Isothermal Fatigue of Interconnections in Flexible Hybrid Electronics Based Human Performance Monitors,” 2018.

[27] R. (Ross) Salary, J. P. Lombardi, P. K. Rao, and M. D. Poliks, “Additive Manufacturing (AM) of Flexible Electronic Devices: Online Monitoring of 3D Line Topology in Aerosol Jet Printing Process Using Shape-From-Shading (SfS) Image Analysis,” no. 50732. p. V002T01A046, 2017.